Drosophila Tropomodulin is required for multiple actin-dependent processes in myofiber assembly and maintenance

Carolina Zapater i Morales[1,2], Peter J. Carman[3,4], David B. Soffar[2], Stefanie E. Windner[2], Roberto Dominguez[3,4], and Mary K. Baylies[1,2,5].

1. Biochemistry, Cell & Developmental Biology, and Molecular Biology (BCMB) program, Weill Cornell Graduate School of Medical Sciences, New York, NY 10065
2. Developmental Biology Program, Sloan Kettering Institute, Memorial Sloan Kettering Cancer Center, New York, NY 10065
3. Biochemistry and Molecular Biophysics Graduate Group, Perelman School of Medicine, University of Pennsylvania, Philadelphia, PA 19104
4. Department of Physiology, Perelman School of Medicine, University of Pennsylvania, Philadelphia, PA 19104
5. Lead contact (Correspondence: bayliesm@mskcc.org)

Keywords: Skeletal muscle, Tropomodulin (Tmod), *Drosophila*, sarcomere length, myofibril orientation, tension-mediating proteins, misshapen nuclei.

SUMMARY STATEMENT

Drosophila Tropomodulin knockdown in larval myofibers results in myopathy-related phenotypes. Our findings support that Tmod acts in actin-related processes at different subcellular locales, all critical for muscle integrity.

ABSTRACT

Proper muscle contraction requires the assembly and maintenance of sarcomeres and myofibrils. While the protein components of myofibrils are generally known, less is known about the mechanisms by which they individually function and together synergize for myofibril assembly and maintenance. For example, it is unclear how the disruption of actin filament (F-actin) regulatory proteins leads to the muscle weakness observed in myopathies. Here, we show that knockdown of *Drosophila* Tropomodulin (Tmod), a F-actin pointed-end capping protein, results in several myopathy-related phenotypes, including reduction of muscle cell (myofiber) size, increased sarcomere length, disorganization and misorientation of myofibrils, ectopic F-actin accumulation, loss of tension-mediating proteins at the myotendinous junction, and misshaped and internalized nuclei. Our findings support and extend the tension-driven self-organization myofibrillogenesis model. We show that, like its mammalian counterpart, *Drosophila* Tmod caps filament pointed ends, and this activity is critical for cellular processes in different locations within the myofiber that directly and indirectly contribute to the maintenance of muscle function. Our findings provide significant insights to the role of Tmod in muscle development, maintenance, and disease.

INTRODUCTION

Skeletal muscle cells, or myofibers, perform many functions essential for survival, including locomotion, breathing, and eating. Myofibers are comprised of myofibrils, each consisting of an array of repeating units known as sarcomeres. Sarcomeres are the fundamental contractile machinery of the muscle, and contain three main structural elements: thin filaments, thick filaments, and Z-discs [reviewed in Sweeney and Hammers (2018)]. Z-discs are the thin filament attachment site and are composed of many proteins, including α-actinin and Zasp. Thin filaments are comprised primarily of actin filaments (F-actin) and actin binding proteins, including proteins important for anchorage to the Z-disc such as CapZ, for contraction such as troponin and tropomyosin, and for F-actin length regulation such as nebulin and tropomodulin (Tmod) [reviewed in Szikora et al. (2022), Ghosh and Fowler (2021), Fowler and Dominguez (2017)]. Thick filaments are composed primarily of myosin and myosin-associated proteins. Sliding of the thin filaments past the thick filaments brings the Z-discs closer together (contraction) and generates force in a calcium-regulated manner. While much is known about the protein composition and function of sarcomeres and myofibrils, critical questions remain regarding the mechanisms controlling their formation and maintenance.

Although myofibrillogenesis is not well understood, the most widely accepted model suggests that tension is essential for this process. According to this model, once the myofiber has attached to tendon cells, short F-actin stochastically attach to each other and to the myofiber ends via tension-activated proteins such as β-Integrin and Talin. Through a positive feedback loop, initial tension attracts more tension-activated proteins, leading to further tension and myofibril assembly and maturation along the longitudinal axis of the myofiber (Lemke and Schnorrer, 2017, Lemke et al., 2019, Pines et al., 2012, Weitkunat et al., 2014, Sparrow and Schock, 2009). Subsequently, tension along the myofibrils is required for additional growth and organization along the long axis of the myofiber (LeGoff and Lecuit, 2015). Several other processes have been implicated in regulating myofibrillogenesis and myofibril maintenance. Firstly, the mechanical interplay between mitochondrial dynamics and myofibril morphogenesis suggests that mitochondria influence myofibrillogenesis and vice versa (Avellaneda et al., 2021). Secondly, myofibrils undergo dynamic protein turnover without compromising their organization during active contraction and myofibrillogenesis (Sanger and Sanger, 2008, Ono, 2010, Littlefield and Fowler, 2008). Finally, actin regulatory proteins that control the ratio of monomeric (G-actin) to F-actin in the cell are thought to be critical for myofibril assembly and turnover (Littlefield and Fowler, 2008,

79 Deng et al., 2021). While some contributing factors of myofibril formation and maintenance have
80 been identified, their interplay and molecular mechanisms are incompletely understood.
81
82 Mutations in sarcomere genes are linked to skeletal muscle diseases such as nemaline myopathy
83 (NM), which presents with defective contraction and muscle weakness (Bonnemann and Laing,
84 2004, Cassandrini et al., 2017, Tubridy et al., 2001, de Winter and Ottenheijm, 2017). NM is
85 associated specifically with mutations in thin filament genes, including ACTA1, NEB, LMOD3,
86 CFL2, TPM2, TPM3, TNNT1, TNNT3 and MYPN [reviewed in Laitila and Wallgren-Pettersson
87 (2021), Christophers et al. (2022)]. In addition to the growing list of mutations identified in human
88 patients, Tmod mutant zebrafish show a NM-like phenotype and muscle weakness (Berger et al.,
89 2014). Studies in a variety of model systems have demonstrated that Tmod is a key component
90 of the thin filament that regulates F-actin length by capping the pointed end to inhibit monomer
91 addition/dissociation (Molnar et al., 2014, Berger et al., 2022, Littlefield et al., 2001). Tmod is also
92 related in sequence and structure to Leiomodin (Lmod), an actin filament nucleator [(Chereau et
93 al., 2008) and reviewed in Fowler and Dominguez (2017), Yamashiro et al. (2012)], whose
94 deficiency has been linked to NM (Yuen et al., 2014, Cenik et al., 2015). Some Tmods also have
95 low nucleation activity (Fischer et al., 2006, Yamashiro et al., 2010, Yamashiro et al., 2014). While
96 humans have four *TMOD* and three *LMOD* genes that cap and nucleate F-actin, respectively,
97 *Drosophila* has no Lmod, but expresses 18 different Tmod splice variants. It is unknown, however,
98 which Tmod isoforms are the most abundant in *Drosophila* muscle and whether individual
99 isoforms cap or nucleate F-actin. It is also unknown whether and how the disruption of Tmod
100 isoforms in *Drosophila* would result in the variety of NM-like defects observed in zebrafish and
101 other organisms.
102
103 Previous studies in muscle mainly focused on the role of Tmod and Lmod in regulating sarcomeric
104 F-actin. However, similar to other cell types, cytoplasmic F-actin plays several essential roles in
105 myofibers: maintenance of intracellular structure by tethering myofibrils to the plasma membrane
106 and the extracellular matrix (ECM), organization of myofiber organelles and vesicle trafficking,
107 and movement and anchoring of myonuclei at the periphery of the myofiber [reviewed in Davidson
108 and Cadot (2021), Charvet et al. (2012), Kee et al. (2009)]. The disruption of cytoplasmic F-actin
109 dynamics could contribute to muscle deterioration and weakness and has not been
110 comprehensively studied. In this work, we analyze the effects of Tmod knockdown (KD) in
111 *Drosophila* larval muscle. We observe progressive muscle deterioration both structural and
112 functional, with defects in muscle size, sarcomere length, myofibril homeostasis, integrin-based

113 myofibril attachment at the muscle ends, and myonuclear shape and activity. In parallel with the
114 breakdown of myofibrillar organization, Tmod KD myofibers show ectopic accumulations of F-
115 actin. Transcriptomic analyses reveal downregulation of proteasomal degradation and
116 upregulation of oxidative metabolism. Biochemically, *Drosophila* Tmod exclusively acts as an
117 actin capping protein which, in addition to regulating thin filament length, plays a critical role in
118 establishing tension along the myofiber. The phenotypes generated by loss of Tmod support and
119 extend the leading hypothesis of myofibrillogenesis and suggest a role for Tmod in myofibril
120 assembly and maintenance. We propose that Tmod's function as an F-actin capping protein is
121 critical in a variety of locations within the myofiber that directly and indirectly contribute to
122 maintaining muscle function.
123

RESULTS

Drosophila Tmod is required for larval muscle integrity

To identify genes with a critical role in muscle development and disease, we performed a limited screen in *Drosophila melanogaster*. We used a muscle-specific driver (*Dmef2-Gal4*) line and available RNAi lines to knock down homologues of human proteins implicated in the regulation of myofibril/sarcomere structure and function (Schnorrer et al., 2010) (Table S1). We screened for embryonic lethality, muscle defects in late third instar larvae (visible by Zasp::GFP, a marker of sarcomeres), pupal lethality, and adult flight (Table S2). Expression of *tmod* RNAi resulted in phenotypes that suggested a critical role in maintaining muscle integrity and function. We confirmed the KD phenotypes using three different RNAi lines and a homozygous *tmod* mutant, and assessed KD levels by qRT-PCR, immunofluorescence, and Western blot analyses (Fig. S1). Based on these results, we selected *tmod* for further study in larval myofibers and used one RNAi line for subsequent KD experiments, dsRNA-HMS02283 (Perkins et al., 2015), as it exhibited an intermediate phenotype and degree of mRNA KD.

The *Drosophila* larva is a segmented organism with three thoracic and eight abdominal body segments (A1-A8), each consisting of a stereotyped pattern of ~30 unique body muscles (Bate, 1990). Here we focused on two ventral longitudinal (VL) muscles, VL3 and VL4 (also known as muscle 6 and 7), which are flat rectangular cells with nuclei located on one cell surface (Fig. 1A-C). These muscles were selected because they are easily assessable and well characterized (Windner et al., 2019). Muscle-specific Tmod KD resulted in a striking phenotype at the end of larval development (late third instar), with a significant reduction in myofiber size (Fig. 1D,E). While the myofiber length was conserved, the width was reduced by 30-60%, resulting in a bone-like shape (Fig. 1D-F). In addition, we observed several distinct morphological features: increased sarcomere length (Fig. 1G), disorganized and misoriented myofibrils (Fig. 1I), ectopic F-actin accumulation (Fig. 1D,E), and misshaped and often internalized nuclei (Fig. 1J). Strikingly, intact and aligned myofibrils with changes in sarcomere length were restricted to the cuticular side of the myofiber. In contrast, the visceral muscle surface, which includes the myonuclei, was completely disorganized (Fig. 1E). These observations supported a crucial function for Tmod in regulating sarcomeric actin and myofibril stability. Furthermore, they suggested additional role(s) of Tmod in the regulation of non-sarcomeric actin, including the stabilization of nuclei and the control of other cellular processes that occur among the nuclei at the myofiber surface.

Tmod KD muscles deteriorate in a specific pattern

158 *Drosophila* larval development can be divided into four stages: first instar, second instar, early
159 third instar and late third instar (the last two hours of this last stage is called the "wandering"
160 stage), during which body wall muscles grow dramatically in size (25 to 40-fold). Over this four-
161 day period, new sarcomeres are assembled, and new myofibrils are added, while nuclear number
162 remains constant (Demontis and Perrimon, 2009, Bai et al., 2007, Balakrishnan et al., 2020). The
163 muscle phenotypes described above were found in Tmod KD late third instar larvae (see also Fig.
164 S1B); however, not all segments throughout the larva were affected equally. Instead, we found a
165 gradient of muscle phenotypes along the larval anterior-posterior (AP) axis. Myofibers in more
166 anterior segments (A1, A2) had severely disrupted myofibrils and nuclei, while posterior ones (A5,
167 A6) maintained nuclear shape and position and exhibited a milder myofibrillar phenotype.
168
169 To further investigate this pattern, we analyzed Tmod KD phenotypes along the larval AP axis
170 and across larval development. In first instar larvae, we observed wildtype (WT)-like muscles,
171 which contained the typical conserved arrays of sarcomeres. The first observed defects in the
172 Tmod KD myofibers were diagonal myofibrils at the myofiber ends of segments A1 and A2 in
173 second instar larvae (Fig. 2A; Fig. S2). At the early third instar stage, these defects also appeared
174 in mid-segments (A4, A5) and became even more pronounced in the anterior segments, which
175 displayed ectopic diagonally intersecting grouped myofibrils (Fig. 2B,D; Fig. S2). At the late third
176 instar stage, the stereotypical myofibrillar pattern was disrupted almost entirely on the visceral
177 side of anterior segments and large bundles of anchored F-actin mostly replaced organized
178 myofibrils (Fig. 2C,F; Fig. S2). Occasionally, interlaced "braided" myofibrils formed at the
179 beginning of late third instar, and ectopic radial F-actin accumulations arose by the end of late
180 third instar (Fig. 2E,G). Additionally, once the first diagonally misoriented myofibrils were observed
181 along a myofiber's long axis, perpendicular myofibrils were found adjacent to the myotendinous
182 junction (MTJ) at the posterior myofiber end (Fig. 2B). These perpendicular myofibrils also later
183 developed at the anterior end of the myofibers (Fig. 2C). Nuclear irregularities also first appeared
184 in anterior segments during late third instar stage and, together with ectopic F-actin structures,
185 were only observed in anterior segments.
186
187 These data suggested that Tmod KD myofibers experience a specific temporal and spatial pattern
188 of structural changes. As the myofibrillar phenotypes progress during larval development, the
189 diagonal misoriented myofibrils are replaced by ectopic F-actin bundles, which suggests these
190 structures are of sarcomeric origin rather than cytoplasmic. The muscle phenotypes appeared in
191 parallel with larval growth, with the most severe disruptions occurring in dramatically growing third

192 instar larvae. In addition, most muscles are larger in anterior abdominal than posterior segments.
193 These correlations indicated that mechanisms of muscle growth and/or homeostasis could be
194 affected in Tmod KD myofibers.
195
196 **Tmod's canonical role as a pointed end capping protein is conserved in *Drosophila***
197 To better understand how loss of Tmod leads to these phenotypes, we studied the biochemical
198 activity of *Drosophila* Tmod using purified proteins *in vitro*. Tmod's canonical role in vertebrates
199 is filament pointed end capping (Dye et al., 1998, Weber et al., 1994, Gregorio et al., 1995,
200 Mardahl-Dumesnil and Fowler, 2001, Fowler and Dominguez, 2017). However, some Tmods also
201 have limited actin filament nucleation activity (Fischer et al., 2006, Yamashiro et al., 2010,
202 Yamashiro et al., 2014), mimicking to some extent the activity of Tmod's structural homolog Lmod
203 that has strong nucleation activity (Chereau et al., 2008). Lmod is not expressed in *Drosophila*.
204 Nonetheless, while mammals express only four Tmod isoforms, *Drosophila* expresses 18 different
205 splice variants. Moreover, several *Drosophila* Tmod isoforms differ substantially in sequence from
206 their mammalian counterparts, displaying N- and/or C-terminal amino acid extensions reminiscent
207 of those present in mammalian Lmods (Fig. S3D). These observations led us to ask whether
208 *Drosophila* Tmod isoforms capped pointed-ends or nucleated filaments.
209
210 Out of the Tmod isoforms that were directly affected by the KD (Fig. S3A-C), we chose two for *in*
211 *vitro* analysis based on sequence analysis and their abundance in control vs. KD muscle. The
212 knockdown strategy targeted transcripts either at the 3'-UTR region or at the last intronic region
213 and reduced the levels of most of the *Drosophila* Tmod isoforms (Fig. S3C). However, the RNAi
214 construct did not target or sufficiently KD three isoforms (A, B, P) (Fig. S3B). Additionally, six
215 isoforms (C, E, G, H, N, R) were either non-detected or were expressed at low levels in control
216 muscle (Fig. S3A). Sequence analysis further showed that all the *Drosophila* Tmod isoforms share
217 an identical central region, displaying strong similarity with mammalian Tmods (Fig. S3D). This
218 region comprises all domains implicated in pointed-end capping, including two Tropomyosin- and
219 two actin-binding sites (Rao et al., 2014). Three of the isoforms have Pro-rich C-terminal
220 extensions (isoforms G, N, R), but these are among the isoforms expressed at low levels and
221 were not further considered (Fig. S3A; Table S3). Thus, we focused on isoforms differing at the
222 N-terminus. Based on their N-termini, the 18 isoforms can be classified into four subgroups; those
223 lacking an N-terminal extension (isoforms A, H) and those displaying extensions of 88 (isoforms
224 D, E, F, G, I, L, M, N, P, Q, R), 58 (isoforms C, J, K, O), and 52 (isoform B) amino acids. Isoforms
225 Q, O, and K, representing two different N-terminal subgroups, had the highest abundance and

226 thus contributed the most to the KD phenotype (Fig. S3A-B; Table S3). These isoforms were
227 chosen for in-depth biochemical analysis (note that isoforms O and K have identical protein
228 sequences).
229
230 We expressed TmodQ, TmodO/K, and human TMOD3 (a control for capping activity) in *E. coli*
231 and purified them using dual N-terminal His and C-terminal Strep affinity tags. We monitored the
232 effect of TmodQ and TmodO/K on actin assembly using the pyrene-actin polymerization assay
233 (Doolittle et al., 2013). Pre-formed F-actin seeds, coated with Tropomyosin and capped at the
234 barbed end with saturating amounts of CapZ, were incubated with varying concentrations of
235 Tmod. Upon addition of G-actin (6% pyrene-labeled), reactions were monitored as the
236 fluorescence increase resulting from the incorporation of pyrene-actin monomers at the pointed-
237 end (Fig. 3, Fig. S3). Because the concentration of actin monomers (1.5 μM) is higher than the
238 critical concentration for monomer addition at the pointed-end (~0.6 μM), pointed-end capping
239 under these conditions would be observed as a decrease in fluorescence with increasing Tmod
240 concentration, resulting from inhibition of monomer addition at the pointed-end. If, on the contrary,
241 Tmod were to nucleate filaments from monomers we would observe an increase in fluorescence
242 (i.e. polymerization), resulting from the formation and elongation of new barbed-ends. Similar to
243 human Tmod3, TmodQ and TmodO/K reduced polymerization in a concentration-dependent
244 manner (Fig. 3A and Fig. S3E-F). These results suggested that the two representative *Drosophila*
245 Tmod isoforms analyzed function as bona fide pointed-end cappers like their mammalian Tmods,
246 and not nucleators like mammalian Lmods. Therefore, the observed KD phenotypes are most
247 likely due to a deficiency in pointed-end capping.
248
249 **Tmod regulates thin filament and sarcomere length**
250 Previous work in different contexts has shown that Tmod regulates sarcomere length by capping
251 the pointed-end of sarcomeric F-actin [reviewed in Littlefield and Fowler (2008), Ghosh and
252 Fowler (2021)]. To assess the effects of Tmod KD in *Drosophila* larval myofibers, we quantified
253 muscle length, Z-disc number, and sarcomere sizes in second and late third instar larvae. We
254 found that at both timepoints Tmod KD myofibers had fewer Z-discs than control myofibers with
255 the same length (Fig. S4). Z-disc numbers were reduced by 15% in the second instar and by 26%
256 in late third instar, indicating that sarcomere size increased in growing Tmod KD myofibers.
257 Accordingly, the distance between Z-discs revealed a significant 22% and 31% increase in
258 sarcomere length in Tmod KD muscles at the second and late third instar stages, respectively
259 (Fig. 3C,D). To confirm that Tmod regulates sarcomere size via its effect on thin filaments, we

260 quantified sarcomeric F-actin length in late third instar larvae. We detected a 35% increase in thin
261 filament length in Tmod KD myofibers. Interestingly, the proportion of thin filament length to
262 sarcomere length was similar to control, whereby thin filaments account for 25% of sarcomere
263 length in both genotypes (Fig. 3B,F). Together these data suggested that the capping of
264 sarcomeric F-actin by Tmod is required to prevent increases in sarcomere size during muscle
265 growth. The same ratio of thin filaments to sarcomere length in Tmod KD and control myofibers
266 further indicates that independent mechanisms maintain sarcomere proportions.
267
268 Sarcomere size is highly conserved for optimal contraction, and changes in its size have been
269 linked to reduced muscle function (Fernandes and Schock, 2014, Molnar et al., 2014, Spletter et
270 al., 2018, Spletter et al., 2015). To assess the functional consequences of muscle-specific Tmod
271 KD, we performed larval locomotion assays. We analyzed larval velocity throughout larval
272 developmental and observed a significant decrease in myofiber function, starting at second instar
273 stage and throughout larval development (Fig. 3E). These data suggest that targeted KD of Tmod
274 caused myofiber weakness even before the appearance of obvious muscle deterioration, and that
275 changes in thin filament length could be the first effect of Tmod KD to reduce muscle function.
276
277 **Tmod stabilizes core components of the muscle attachment site**
278 The current model of sarcomere assembly and myofibrillogenesis suggests that tension is crucial
279 for this process. Specifically, the muscle attachment sites at the MTJs play a fundamental role in
280 generating tension within a myofiber. The MTJ represents an analogous structure to focal
281 adhesion sites (Atherton et al., 2016, Martino et al., 2018, Pardo et al., 1983, Quach and Rando,
282 2006, Mohammad et al., 2012), which are composed of the Vinculin-Talin-Integrin complex
283 tethering the actin cytoskeleton to the ECM, or in the case of the myofiber, the myofibrils to the
284 muscle attachment site. We hypothesized that Tmod could function at the MTJs to generate the
285 myofibril phenotypes that we observed.
286
287 In accordance with this hypothesis, we detected Tmod protein localized at the ends of control
288 myofibers, adjacent to myofibrillar F-actin and co-localizing with β_{PS}-Integrin (Mys) (Fig. 4A,C). To
289 determine if myofibril attachment was affected in Tmod KD myofibers, we evaluated protein levels
290 of the tension-mediating proteins β_{PS}-Integrin and its binding partner Talin (Rhea). Our
291 quantifications in second and late third instar larvae indicated a significant decrease of β_{PS}-
292 Integrin and Talin at Tmod KD MTJs in anterior segments (Fig. 4E,F; Fig. S5A-C), however we
293 did not detect detachment of myofibers. To determine whether the strong decrease in signal was

294 due to mislocalization or an overall decrease in protein levels, we performed Western blot
295 analysis. Tmod KD muscle lysates did not show a decrease in Talin levels in late third instar larvae
296 (Fig. 4B), suggesting that Talin is mislocalized. Upon further examination of the immunolabelling
297 experiments, we observed pools of enriched β_{PS}-Integrin and Talin in ectopic areas (Fig. 4F).
298 These data suggest the actin capping function of Tmod is required for establishing the proper
299 anchorage sites at the myofiber ends by stabilizing the interaction between F-actin filaments and
300 tension-mediating proteins.
301
302 To address whether mislocalization of β_{PS}-Integrin and Talin correlated with a loss of tension at
303 the MTJ, we labelled for phospho-tyrosine (pTyr), a marker of active cytoskeletal tension sites
304 (Chrzanowska-Wodnicka and Burridge, 1994, Martino et al., 2018, Parsons et al., 2010). We
305 observed a significant decrease in pTyr labeling at Tmod KD MTJs (Fig. 4F; Fig. S5D), indicating
306 reduced tension at these attachment sites. Together, these experiments suggested a decrease
307 in mechansensory proteins and a reduction of tension at the muscle ends. A lack of tension could
308 cause myofibrillar disorganization and impaired myofibrillogenesis in the Tmod KD myofibers.
309
310 **Tmod plays a role in myonuclear morphology, positioning, and function**
311 Cytoplasmic actin filaments are found in and around the nucleus (Davidson and Cadot, 2021,
312 Caridi et al., 2019). These filaments play roles in gene expression, in the cell's response to
313 mechanical stimuli, and in nuclear positioning in several systems (Farina et al., 2016, Verheyen
314 and Cooley, 1994, Chang et al., 2015). We hypothesized that Tmod KD could affect cytoplasmic
315 F-actin to generate the nuclear phenotypes that we observed. Control *Drosophila* larvae displayed
316 multiple, evenly spaced, round disc-shaped and linearly organized nuclei on the visceral side of
317 each myofiber. In contrast, many Tmod KD nuclei were elongated, with an increased perimeter
318 compared to control (Fig. 5A-C). Along the longitudinal cell axis, the most irregular shaped nuclei
319 were located towards the middle of the myofiber (Fig. 5D). It is possible that Tmod KD directly
320 affected F-actin dynamics that stabilize nuclear shape and position. Unfortunately, imaging of
321 cytoplasmic or nuclear F-actin in myofibers is obstructed by the bright signal of the underlying
322 sarcomeres, which prevented the further analysis of direct effects of Tmod KD on cytoskeleton
323 and nucleoskeleton in this study.
324
325 In myofibers, stable radial microtubule (MT) arrays around the nuclei are key for maintaining
326 positioning and nuclear integrity during contraction (Zheng et al., 2020, Becker et al., 2020,
327 Manhart et al., 2018, Metzger et al., 2012). In addition, MTs are known to physically interact with

328 actin (Farina et al., 2016, Dogterom and Koenderink, 2019), which raises the possibility that actin-
329 MT crosstalk is involved in maintaining nuclear shape and position. To assess if perinuclear MTs
330 were affected in Tmod KD muscles, we quantified the number of intact radial MT arrays in control
331 and Tmod KD myofibers. We observed a significant decrease in intact perinuclear MT arrays in
332 Tmod KD muscles and noted a decrease in longitudinal MT-tracks when compared to controls
333 (Fig. 5E; Fig. S6A). These data indicated that Tmod affects critical MT networks in myofibers, by
334 mediating, we suggest, the interactions of the MT cytoskeleton with actin filaments in/around the
335 nuclei. A loss of perinuclear MTs could subsequently result in destabilization of nuclear shape
336 and position.
337
338 To test if nuclear activity was affected by changes in nuclear morphology, we analyzed the
339 transcriptional and translational potential of Tmod KD myonuclei. To assess transcription, we
340 quantified immunolabeling of H3K9ac, a marker of open chromatin and transcriptionally active
341 regions in the DNA. This analysis revealed that nuclei with the most irregular shapes (below 0.6
342 roundness) exhibited decreased H3K9ac levels, whereas WT-shaped nuclei (above 0.6
343 roundness) showed similar H3K9ac levels to control (Fig. 5F,H; Fig. S6B). To assess translation,
344 we quantified nuclear labeling intensity of Fibrillarin (Fib), a nucleolar protein that plays an
345 essential role in ribosome biogenesis and is a commonly used marker for protein synthesis
346 (Gillery et al., 1996, Lefevre et al., 2001). We found that misshaped nuclei (below 0.6 roundness)
347 exhibited similar Fib intensity levels to control nuclei, while WT-shaped nuclei (above 0.6
348 roundness) showed higher levels than controls (Fig. 5G,I; Fig. S6C). These data suggested that
349 loss of nuclear shape and position in Tmod KD myofibers reduced transcriptional output but
350 increased translational potential. While deformed nuclei are functionally compromised, WT-
351 shaped nuclei in the Tmod KD muscle appeared to compensate for this deficiency by increasing
352 translation.
353
354 **Tmod KD affects actin isoforms, proteasomal degradation, and oxidative metabolism**
355 To better understand the mechanisms behind the observed phenotypes and uncover additional
356 effects of Tmod KD, we analyzed the transcriptome of Tmod KD larvae. Consistent with the
357 morphological features found in Tmod KD muscle, we detected misregulation of actin genes. For
358 example, the sarcomeric actin isoforms (Act57B and Act87B) (Roper et al., 2005, Fyrberg et al.,
359 1983) were upregulated (Fig. 6; Table S4) in accordance with the ectopic F-actin bundles that we
360 observe (Fig. 2, 6E), which supports a sarcomeric origin for these structures. In contrast,
361 cytoplasmic actin isoforms (Act5C and Act42A) were downregulated in Tmod KD myofibers (Fig.

362 6E; Table S4), consistent with the alterations in nuclear shape detected in Tmod KD. We also
363 performed an over-representation analysis (ORA) to determine if a set of shared genes was
364 differentially expressed based on Gene Onthology (GO) and Kyoto Encyclopedia of Genes and
365 Genomes (KEGG) gene sets. The data indicated that degradation-related genes (particularly
366 proteasomal genes) and/or pathways were downregulated, while metabolism-linked genes
367 (particularly oxidative metabolism genes) and/or pathways were upregulated in Tmod KD larvae
368 (Fig. 6A,B). Specifically, we observed upregulation of mitochondrial metabolism genes from both
369 glycolysis and oxidative phosphorylation. However, genes involved in oxidative metabolism and
370 linked to ATP production were particularly enriched. To test whether ATP production was indeed
371 altered in Tmod KD muscles, we performed a functional ATPase assay. Consistent with our
372 RNAseq data, we observed that ATP levels were significantly increased in Tmod KD myofibers
373 by at least 2-fold (Fig. 6C). Together, these data suggest a role for Tmod, either directly or
374 indirectly, in gene expression. We speculate that these changes reflect a compensatory
375 mechanism to promote growth in a degenerating muscle.
376
377

378 **DISCUSSION**

379 Tmod function in the actin cytoskeleton has been studied using various cell types, including in the
380 sarcomere of myofibers (Fowler, 1997). Here we investigated the effects of Tmod KD in
381 *Drosophila* larval myofibers during development using a combination of detailed *in vivo* analyses,
382 *in vitro* experiments, and transcriptomic approaches. Tmod KD muscles exhibit: (1) increased
383 thin filament and sarcomere length; (2) reduced tension at the cell ends, disorganized myofibrils
384 and impaired myofibrillogenesis; (3) ectopic accumulation of non-sarcomeric F-actin; and (4)
385 misshaped and internalized nuclei with impaired function. In addition, our data show an
386 enrichment of metabolism-linked genes and ATP production, and decreased expression of
387 degradation-linked genes. Together, our studies suggest that through its capping function, Tmod
388 affects actin dynamics in different locations within the muscle fiber and is ultimately essential for
389 muscle function.

390

391 We propose the following model for Tmod's pleiotropic effects in muscle cells (Fig 7). In the
392 sarcomere, the barbed end of F-actin is capped by CapZ and anchored to the Z-disc, while the
393 pointed-end is capped by Tmod. However, due to Tmod's low affinity for F-actin, there are yet
394 opportunities for monomer addition and therefore, the pointed-end remains suitable for sarcomere
395 growth. When Tmod is removed, thin filaments grow in length, consistent with other studies. We
396 suggest that this additional polymerization would cause sufficient imbalance to favor the
397 production of muscle-specific larval G-actin isoforms (Act57B and Act 87E); this increased G-actin
398 availability and continuously growing sarcomeric F-actin would lead to the formation of ectopic F-
399 actin bundles and radial F-actin structures. In the cytoplasm, actin filament growth occurs through
400 the canonical pathway, which is, generally, by the addition of G-actin monomers at the barbed
401 end and depolymerization at the pointed-end. When Tmod is reduced, excessive
402 depolymerization occurs, due to loss of Tmod's capping activity. This excess of G-actin monomers
403 decreases the production of cytoplasmic-specific actin isoforms (Act5C and Act42A). Loss of
404 cytoplasmic perinuclear and nuclear F-actin would then contribute to the loss of nuclear
405 organization and directly or indirectly affect nuclear output. At the MTJ, myofibrils are anchored
406 to the muscle ends via cytoplasmic F-actin. In the absence of Tmod, lack of stable attachments
407 via F-actin impairs tension along the myofibrils, leading to myofibril disorganization and
408 deterioration, and defects in myofibrillogenesis. Protein degradation and metabolism would be
409 affected in a similar way: destabilization of required structures for myofiber organization or via
410 transcriptional changes. Together, loss of Tmod at these different sites leads to the deterioration
411 in muscle function.

412 While every muscle cell in our system experiences the same Tmod KD effect and follows the
413 same pattern of deterioration, not every myofiber is affected equally. Along the larval AP axis, we
414 see that the *tmod* phenotypes appear first and are most severe in anterior abdominal segments,
415 a phenotype that has not been reported previously to our knowledge. In general, muscles in more
416 anterior abdominal segments are larger than in posterior ones, suggesting that growth and/or
417 myofiber size may be a contributing factor. However, we observe that some muscles at the same
418 axis position are preferentially affected, which suggests a more complex situation. Freely moving
419 *Drosophila* larvae constantly pivot and sweep their heads, movements which are mainly
420 supported by muscles of segments A1, A2 and A3 (Lahiri et al., 2011); hence, muscle usage may
421 affect muscle deterioration in our model. In parallel with this study, the timing and distribution of
422 muscle pathology in many human muscle diseases, as well as animal models, follow specific
423 patterns (Barohn et al., 2014, Sewry et al., 2019). Studies in vertebrate models suggest that
424 muscle fiber type might play a role [reviewed in Talbot and Maves (2016)]. The factor, or more
425 likely combination of factors, that make specific muscles more susceptible to muscle deterioration
426 remain unknown. The *Drosophila* larval musculature, consisting only of one fiber type, provides a
427 useful system for further studies in this context.
428
429 Alternative splicing result in a total of 18 Tmod isoforms. Why the fly produces so many different
430 isoforms is unclear. In this study we biochemically tested two isoforms which were chosen as
431 representatives from the major classes identified using sequence alignment and based on their
432 expression profile in RNAseq experiments. We show that isoforms TmodQ and TmodO/K display
433 Tmod's characteristic F-actin capping function, despite having N-terminal extensions comparable
434 to the human TMOD isoforms. We did not find any biochemical evidence of F-actin nucleation,
435 and the phenotypes observed in Tmod KD myofibers did not indicate defects in F-actin nucleation.
436 It is possible that one of the remaining Tmod isoforms (most notably the isoforms with C-terminal
437 proline-rich extensions) may possess nucleation activity like that of human Lmods. However, the
438 extremely low levels of such isoforms in our RNAseq data would suggest they are not expressed
439 in this cell type, or at the development stages tested.
440
441 Tmod has been suggested to play a key role in defining thin filament and sarcomere length in a
442 variety of model systems (Szikora et al., 2022). In adult *Drosophila*, Tmod overexpression results
443 in shorter sarcomeres (Molnar et al., 2014). In vertebrate systems, such as mouse Tmod-null
444 mutants, thin filament length is increased (Littlefield and Fowler, 2008). Prior *in vitro* research in
445 rat cardiomyocytes showed that adenoviral expression vectors that increase or decrease Tmod

446 levels result in shorter or longer sarcomeric actin filaments, respectively (Sussman et al., 1998).
447 Our data demonstrate that Tmod KD in *Drosophila* larval myofibers increases thin filament and
448 sarcomere length. The ratio of thin filament to sarcomere length was maintained in Tmod KD
449 myofibers. This ratio was similar to measurements taken from the frog sartorius (26%) and the
450 human pectorialis (30%) while at maximum sarcomere length (Gokhin and Fowler, 2013). This
451 indicates that mechanisms that regulate sarcomere proportions are conserved and regulated
452 independently of Tmod function. We further find that sarcomere sizes increase over the course of
453 larval growth, indicating that the uncapped pointed-ends of sarcomeric actin filaments do not
454 respect a specified size, exhibiting continuous polymerization in the absence of Tmod.
455 Furthermore, we show an inverse relationship between sarcomere number and sarcomere length
456 in Tmod KD myofibers that suggests that myofibrils can grow by increasing their length via
457 sarcomere growth instead of sarcomere addition in this context. Our data are consistent with
458 recently published work that indicated that muscle length and sarcomere number are regulated
459 independently of one another (Brooks et al., 2022). In healthy muscle, sarcomere length is fixed
460 to optimize muscle contraction, forcing growing cells to add sarcomeres rather than increasing
461 their length (Balakrishnan et al., 2020, Williams and Goldspink, 1971, Dix and Eisenberg, 1990,
462 Goldspink, 1983, Haas, 1950). Loss of this adaptive behavior is associated with myopathy
463 progression (Ottenheijm et al., 2009, Winter et al., 2016). Moreover, the decrease in myofiber size
464 is suggestive of compromised myofibril addition to increase muscle mass, which further supports
465 that mechanisms of muscle growth – addition of new sarcomeres and hypertrophy– are affected
466 in Tmod KD larva. Our analyses show locomotive defects (first instar stage) before discernable
467 changes in myofiber structure and morphology (second instar). While technical limitations
468 prevented the detailed analysis of first instar sarcomeres, we suggest that changes in thin filament
469 length might be the first effects of Tmod KD that directly affect muscle function. In parallel with
470 disruption of sarcomeres and myofibrils, Tmod KD myofibers display accumulation of ectopic and
471 disorganized F-actin. The location of these ectopic radial F-actin accumulations and filament
472 bundles near disorganized myofibrils indicates that continuously growing thin filaments could
473 contribute to these ectopic structures. Whether the ectopic disorganized F-actin filaments were
474 intended to serve as a myofibril template (Fenix et al., 2018, Dlugosz et al., 1984) or they result
475 from deteriorating myofibrils remains unclear.
476
477 The currently favored hypothesis in the field describes sarcomere and myofibril formation as a
478 tension-driven self-organizing process, whereby the tension that is generated through muscle
479 attachment at the MTJs is used to orient and longitudinally assemble sarcomeres and myofibrils

480 (Lemke and Schnorrer, 2017). Here, we show that Tmod KD results in mislocalization of two core
481 mechanosensitive proteins (β_{PS}-Integrin, Talin), and a reduction in tension (pTyr) at the muscle
482 ends. According to the hypothesis, lack of tension at the muscle ends could affect addition of new
483 sarcomeres as well as homeostasis along the entire myofibril. This is consistent with our
484 experiments, showing reduced number of sarcomeres, and aberrant myofibril organization and
485 stability in Tmod KD myofibrils. Previous studies using *Tmod* mutant zebrafish also reported
486 defects in myofibril organization and muscle weakness (Berger et al., 2022, Berger et al., 2014),
487 but a role for Tmod in sarcomere addition had not been described. An interesting observation in
488 our study is the perpendicular myofibrils exclusively localized at the myofiber ends, which
489 demonstrate sarcomeric organization albeit incorrect orientation. In vertebrate and *Drosophila*
490 muscles, the ends of the myofibers are considered sites of muscle growth where newly formed
491 sarcomeres are added (Balakrishnan et al., 2020, Bai et al., 2007). This raises the possibility that
492 due to the lack of longitudinal stability in this growth zone, the forming sarcomeres and growing
493 myofibrils orient towards the next best structure that provides resistance, connecting to existing
494 myofibrils or the visceral plasma membrane. A similar phenotype with misoriented myofibrils was
495 observed in *Drosophila* larval muscle expressing the constitutively active form of C3G, a Rap1
496 activator (Shirinian et al., 2010). Importantly, Rap1 has been demonstrated to recruit Talin to the
497 cell membrane (Shattil et al., 2010, Lee et al., 2009). We find ectopic localization of
498 mechanosensitive proteins along the plasma membrane of Tmod KD myofibers, which could lead
499 to ectopic F-actin accumulations. This could result in local changes in tension throughout the
500 myofiber and contribute to myofibril misalignment. Together, our study suggests that Tmod is
501 crucial for maintaining organization and stability as well as for growth and alignment of myofibrils.
502 Our data are consistent with the tension-driven self-organizing myofibrillogenesis hypothesis and
503 supplements this model by suggesting a role for Tmod in tension mediation. It is unclear, however,
504 if Tmod directly interacts with β_{PS}-Integrin and/or Talin or if it acts indirectly via stabilizing F-actin.
505
506 Our data suggest a role for Tmod in nuclear positioning in the Z-axis and in maintaining nuclear
507 morphology. Mispositioned and deformed nuclei are common in many myopathies including
508 nemaline myopathy, centronuclear myopathy and laminopathies (Romero, 2010, Steele-Stallard
509 et al., 2018, Ross et al., 2019), highlighting the relevance of correct nuclear positioning for proper
510 muscle function. Actin has been previously shown to play a structural role in the nucleus (Bettinger
511 et al., 2004), making it possible that Tmod, through its capping function, stabilizes nuclear and/or
512 perinuclear actin and therefore directly supports nuclear integrity. We did not detect nuclear or
513 perinuclear actin filaments, possibly due to the strong F-actin signal of the adjacent thin filaments.

514 However, we found defects in the MT networks surrounding the nuclei of Tmod KD myofibers. It
515 is well known that MTs play a crucial role in myonuclear positioning and integrity, and that they
516 interact with actin filaments. Thus, it is likely that Tmod KD has indirect effects on myonuclei by
517 disrupting actin-MT interactions. In addition, defects in nuclear positioning and morphology could
518 be indirectly affected by the loss myofibril structure and orientation. In Tmod KD myofibers, nuclei
519 are initially located at the periphery, but subsequently sink as myofibril structure is lost. Force
520 exertion on the internalized nuclei could then lead to deformation of nuclear shape. These nuclei
521 also show defects in transcriptional activity. Interestingly, WT-shaped nuclei in Tmod KD myofibers
522 display increased translation makers, consistent with a compensatory mechanism. In addition to the
523 effects of nuclear morphology, it is possible that Tmod plays a role in transcription and/or translation
524 via its effect on actin dynamics. G-actin has many important functions in the nucleus and nucleolus
525 and directly regulates gene transcription (Visa and Percipalle, 2010, Bettinger et al., 2004). More
526 research is needed to determine how deviation from normal positioning in 3 dimensions (X,Y,Z
527 planes) results in impaired muscle function: to this end, future studies focused on the distribution
528 of gene products throughout the muscle cell in contexts where nuclear positioning is aberrant
529 would be informative.
530
531 Our transcriptome analyses suggest that Tmod KD affects two main processes, degradation and
532 mitochondrial metabolism, which are key for myofiber growth (Schiaffino et al., 2013). However,
533 the decrease in degradation and increase in mitochondrial metabolism detected in *tmod* KD
534 myofibrils is inconsistent with impaired muscle growth and muscle weakness that we observe.
535 We suggest that this transcriptomic profile indicates a compensatory attempt of the myofibers to
536 grow and possibly correct the lack of tension along the myofiber, despite structural deterioration.
537 It is possible that the presence of actin inside the nucleus causes these changes through structural
538 and/or transcriptional changes (Chase et al., 2013, Visa and Percipalle, 2010). However, similar
539 myofiber phenotypes and changes in metabolism have been observed in *Drosophila TRIM32*
540 (*thin*) mutant larval muscles (LaBeau-DiMenna et al., 2012, Bawa et al., 2020). Loss of *Drosophila*
541 *TRIM32,* an E3-ubiquitin ligase, resulted in a decrease in glycolytic intermediates, indicating that
542 TRIM32 switches the metabolism from oxidative to glycolytic. The mechanisms by which Thin and
543 Tmod are connected remain to be elucidated, yet the similarities in phenotype and transcriptome
544 suggests they might be interacting genetically or biochemically. This would indicate a role for
545 Tmod in dampening oxidative metabolism and, therefore, ATP production. Strikingly, structural
546 components involved in these pathways, such as mitochondria, are located in high densities at

547 the visceral muscle surface, surrounding the muscle nuclei, indicating that they could be affected
548 indirectly via the destabilization of the underlying myofibrils.
549
550 Myopathies are often devastating disorders characterized by impaired muscle function that are
551 frequently associated with sarcomeric mutations. The molecular details underpinning this
552 relationship are poorly understood. Our study shows a series of phenotypes associated with KD
553 of one critical thin filament component, Tmod, that reach far beyond the sarcomere. Our findings
554 have important implications, as they suggest a key role for Tmod in several cellular processes,
555 including the regulation of actin isoform expression, the stabilization of tension-mediating proteins,
556 and nuclear integrity and positioning, therefore providing additional insight to the pathogenesis of
557 myopathies. The mechanisms directly linking Tmod and critical myofiber processes, including
558 proteasomal degradation and oxidative metabolism, remain to be fleshed out. Furthermore, our
559 findings support and strengthen the tension-driven self-organizing myofibrillogenesis model.
560 Taken together, this study adds significantly to the understanding of the role of Tmod in both
561 muscle development, maintenance, and disease, making it a potential target for new therapeutics
562 that address muscle weakness.
563
564

565 **METHODS**

566 ***Drosophila* husbandry, stocks and crosses**

567 *Drosophila* stocks and experimental crosses were grown on standard cornmeal medium at 25ºC
568 in 12:12 Light:Dark conditions under humidity control. The Gal4-UAS system (Brand and
569 Perrimon, 1993) was used for RNA interference studies. Details on the screen that lead to our
570 analysis of *tmod* are found in Table S1 and S2. For muscle-specific expression and RNAi
571 potentiation we tested different driver lines (*UAS-dicer2;;Mhc-Gal4,Zasp66::GFP*, *UAS-*
572 *dicer2;;Dmef2-Gal4,Zasp66::GFP/Tm6,Hu,Tb* and *UAS-dicer2;;Dmef2-Gal4/Tm6,Hu,Tb*) in
573 combination with *3 UAS-tmod-RNAi* lines (BDSC#41718, BDSC #31534 and VDRC #108389) to
574 validate on-target effects and explore KD levels. The driver lines were crossed with *UAS-*
575 *mCherryRNAi* (BDSC #35785) as the *control RNAi.* In all instances, larvae displaying a Tb
576 phenotype (indicatory of balancer chromosome) were excluded from the F_1 analyzed. The mutant
577 stock $tmod^{MI02468}$ (BDSC #36446) was also used for phenotype validation with *yw* as control.
578 Except where specified, we used a Dmef2-Gal4 driver and one *UAS-tmodRNAi* line
579 (BDSC#41718) for analyzing Tmod KD phenotypes (the line is referred to as "*tmod"*). Table S5
580 contains details on fly stocks.

581

582 **Larval staging**

583 For all larval experiments, larvae were kept at 25ºC and both male and female larvae were
584 analyzed. Staging was performed on apple juice agar plates, either in the embryo (see Viability
585 assay), or by selecting larvae hatched within a 2h period. First instars intended for experiments
586 were maintained in an apple juice agar plate with yeast paste for ease of manipulation. Larvae for
587 experiments at later stages (locomotion, muscle analysis) were transferred to standard food vials.
588 Larvae were removed from food vials using 30% sucrose solution at second instar stage (~24h
589 after transfer), early third instar (~48h after transfer), late third instar (~96h after transfer) and
590 wandering (~118h after transfer) stage. Myofiber structure time-course analysis was performed
591 on all four distinct larval stages, in VI1 or VL3/VL4 muscles of anterior segments (A1 and A2). For
592 the RNAseq experiment, late third instars (~90h after transfer) were processed for dissection. For
593 all other experiments at late third instar stage (~3.5 days), staging was confirmed by using
594 developmental landmarks such as mouth hooks, and spiracle morphologies (Bodenstein, 1950).

595

596 **qRT-PCR**

597 Ten third instar wandering larvae were dissected and rinsed in ice cold HL3.1 medium (Feng et
598 al., 2004) as described in (Brent et al., 2009). Total RNA was extracted from the muscle enriched

599 larval fillets using TRIzol reagent (ThermoFisher #15596026), followed by cleanup with TURBO
600 DNA-free Kit (Ambion #AM1907). The SuperScript III First-Strand Synthesis System for RT-PCR
601 (Invitrogen #18080-051) was used to synthesize cDNA and qRT-PCR reactions were performed
602 on the BioRad CFX96 Real-Time PCR system using the SYBR Select Master Mix for CFX
603 (Applied Biosystems #4472937). Three independent mRNA preparations per genotype were
604 collected and were run in triplicate. Fold changes were calculated based on values obtained using
605 the delta-delta Ct method (Livak and Schmittgen, 2001, Schmittgen and Livak, 2008). Product
606 size and uniformity was assessed via melt curve analysis. *Rpl32* was used as a normalization
607 control. Table S3 contains details on the oligonucleotides used.
608
609 **Western Blot**
610 Seven to ten late third instar wandering larvae were dissected (See Immunolabeling and Imaging)
611 and transferred into larval lysis buffer (50mM HEPES pH 7.5, 150mM NaCl, 0.5% NP40, 0.1%
612 SDS, 2mM DTT) supplemented with Complete mini protease inhibitor cocktail [one tablet in 10mL
613 of lysis buffer (Roche #11836153001)]. Lysates were homogenized and protein concentrations
614 were determined using the Bradford assay. Equal amounts of protein (20 μg) were run on a 5%
615 (Talin) or 10% (Tmod) polyacrylamide gel and then transferred onto a nitrocellulose membrane
616 (ThermoScientific #88018). Membranes were blocked with either 5% milk or 5% BSA in TBST
617 (Tris-Buffered Saline +0.1% Tween) for 1h at room temperature. Table S5 contains details on
618 primary and secondary antibodies. Immunoreactions were visualized in a KwikQuant Imager
619 (Kindle Biosciences, LLC #D1001) using 1-Shot Digital-ECL (Kindle Biosciences, LLC #R1003)
620 and intensities were quantified using Fiji (NIH). Protein expression was normalized to GAPDH
621 (loading control) within each sample. Figures and quantifications are representative of 3
622 experiments.
623
624 **Larval tracking**
625 Larvae were staged and extracted from food vials (see Larval staging) at first instar, second instar,
626 early third instar, and late third instar. One larva at a time was placed at the center of an apple
627 juice agar plate (8.5cm diameter) and recorded for 45 seconds (Samsung Galaxy S8+). Movies
628 were converted into image sequences (1 image per second) and each larva was tracked using
629 the Manual Tracking plug-in on Fiji. Average velocity was calculated as in (Balakrishnan et al.,
630 2021). For each genotype, we performed three replicates with ~10 larvae each. Larval length was
631 equivalent in both phenotypes for each developmental stage.
632

633 **Plasmids**

634 The cDNA for TmodO/K (NCBI Reference Sequences: NP_001247373.1 / NP_001189319.1) was
635 acquired from DNAsu clone DmCD00765633 (Tempe, AZ, USA). The cDNA for TmodQ (NCBI
636 Reference Sequence: NP_001263112.1) was synthesized by GeneWiz (South Plainfield, NJ,
637 USA). Each cDNA was PCR-amplified and ligated between the SacI and KpnI sites of
638 pRSF_Duet1 (Millipore Sigma, Burlington, MA, USA) with an N-terminal 6x histidine tag and a C-
639 terminal Strep-II tag.

640

641 **Protein expression and purification**

642 Tmod isoforms in pRSF_Duet1 were expressed in ArcticExpress(DE3) RIL cells (Agilent
643 Technologies), grown in Terrific Broth (TB) medium for 6 h at 37 °C to an optical density of ~1.5
644 at 600 nm (OD600), followed by 24 h at 10°C in with 0.4 mM isopropyl-β-D-thiogalactoside (IPTG).
645 Cells were harvested by centrifugation (4,000g), resuspended in nickel buffer (20 mM HEPES pH
646 7.5, 300 mM NaCl, 10 mM imidazole, 1 mM PMSF), and lysed using a microfluidizer apparatus
647 (Microfluidics). Proteins were first purified on nickel-NTA resin, washed with 20 column volumes
648 of nickel buffer, and eluted using nickel buffer supplemented with 300mM imidazole. Elution
649 fractions containing the Tmod proteins were then loaded onto Streptactin XT resin (IBA Life
650 Sciences, Göttingen, Germany) and washed with 20 column volumes of strep buffer (20 mM
651 HEPES pH 7.5, 150 mM NaCl, 1 mM EDTA). Proteins were eluted using strep buffer
652 supplemented with 40mM biotin, and further purified through a SD200HL 26/600 gel filtration
653 column (GE Healthcare) in strep buffer supplemented with 1 mM DTT. Human CapZ (Rao et al.,
654 2014), rabbit skeletal muscle actin (Pardee et al., 1982), and rabbit skeletal muscle tropomyosin
655 (Smillie, 1982) were purified as described.

656

657 **Pointed-end capping assay**

658 Capping assays were carried out as described previously (Rao et al., 2014, Kumari et al., 2020).
659 Briefly, 1.5 μM G-actin (6% pyrene-labeled), 1.5 μM F-actin seeds, 25 nM CapZ, and 1 μM
660 tropomyosin were assayed alone or with Tmod at 4 different concentrations (25, 100, 400, 800
661 nM). Pyrene fluorescence (excitation 365 nm, emission 407 nm) was detected using a plate
662 reader (BioTek Cytation 5), and for each Tmod concentration four replicates were recorded.
663 Maximum polymerization rates were determined by taking the first derivative of each curve,
664 identifying the time interval corresponding to the greatest slope, and performing a linear
665 regression on the original data within that time interval.

666

667 **Immunostaining and confocal imaging**

668 Larvae were dissected in ice cold HL3.1 medium as described in (Brent et al., 2009) and fixed
669 with 10% formalin (Sigma-Aldrich #HT501128) for 20 minutes. Larval filets were blocked with
670 PBT-BSA [1x PBS supplemented with 0.3% Triton X-100 (Sigma-Aldrich #X100) and 0.1% BSA
671 (Sigma-Aldrich #A7906)] for 30 minutes. Larval filets were then incubated with primary antibody
672 (Table S5) overnight at 4ºC, followed by washes in PBT-BSA. Incubation with Alexa Fluor-
673 conjugated secondary antibodies (Table S5), Phalloidin and/or Hoechst 3342 were performed at
674 room temperature for 2 hours, followed by washes in PBT. Subsequently, larval filets were
675 mounted in ProLong Gold (Invitrogen #P36930) and slides were cured at room temperature for
676 24h. Z-stacks were acquired using a SP5 laser-scanning microscope (Leica Microsystems) with
677 either dry objectives (HC PL APO CS 10x/0.40 and HC PL APO CS2 20x/0.75) or oil-immersion
678 objectives (HC PL APO CS 20x/0.70, HCX PL APO CS 40x/1.25-0.75, HCX PL APO CS 63x/1.40-
679 0.60, and HCX PL APO CS 100x/1.46). All samples intended for direct comparison were imaged
680 using the same confocal settings. Maximum intensity projections of confocal Z stacks were
681 rendered using Fiji. Approximately 7 larvae (range: 5-10) of each genotype were dissected and
682 experiments were repeated at least twice.

683

684 **Quantification of muscle defects per segment**

685 Muscle defects in second instar, early third instar, and late third instar larvae were scored based
686 on ectopic and abnormal actin structures using a confocal microscope. A score was given for
687 each VL3/4 muscle pair: 3 – WT-like, 2 – mild structural defects (diagonal myofibrils) and 1 –
688 severe defects in muscle structure. We evaluated muscles in both hemisegments of the larva in
689 abdominal segments 1-6. This analysis was performed in triplicate with 3-4 larvae per replicate.

690

691 **Sarcomere and thin filament size/count analysis**

692 Larvae expressing a Zasp::GFP protein trap were fixed by brief (~5 seconds) submersion in 65°C
693 water and mounted on a slide with halocarbon oil. Z-stacks of the cuticular side of the VL3 or VL4
694 muscles from abdominal segment 2 were acquired using a SP5 laser-scanning microscope (Leica
695 Microsystems) with either a HC PL APO CS2 20x/0.75 (late third instars) or HCX PL APO CS
696 40x/1.25-0.75 (second instars) oil immersion objective.

697

698 Muscle length, sarcomere size and number were quantified as described in step 32 of
699 (Balakrishnan et al., 2021). For accuracy and to assess potential regional differences, sarcomere
700 size was also quantified by an alternative method. Z-stacks were opened in Fiji and a line that

701 spanned six Z-discs (five sarcomeres) was made using the line tool. Subsequently, the line
702 intensity plot was obtained, and the X-coordinates (microns) of the peaks were acquired with the
703 multi-point tool. The distance in microns between Z-disks was obtained by calculating the
704 difference between the X-coordinates of the six peaks. This analysis was done in triplicate. In
705 each replicate, six muscles were analyzed, each belonging to an individual larva. Three lines were
706 traced per muscle: in the anterior fraction of the muscle, in the medial region and in the posterior
707 end, with a total of ~90 sarcomere size measurements per replicate (Fig. S4C).
708
709 Sarcomere length was obtained from Zasp::GFP heat-fixed larvae, which was performed by a
710 direct method from Z-disc to Z-disc distance. Due to technical challenges in some areas of the
711 muscles, two confirmatory methods were also employed. First, measurements were confirmed by
712 comparing the heat-fixed samples with a formalin fixed sample. Second, we performed a
713 sarcomere length average by taking the muscle length divided by the total number of Z-discs.
714
715 Thin filament length was assessed in formalin fixed samples that displayed a clear striation pattern
716 and a clear M-line (therefore, we conclude the muscles were in a stretched configuration). Zasp
717 was used as a marker for Z-discs, we traced a line spanning three contiguous Z-discs. The line
718 intensity plot of Phalloidin was obtained and was normalized by calculating deviation from the
719 mean to account for background noise; those with values above zero were used to calculate thin
720 filament length.
721
722 **Intensity quantification at the muscle ends (MTJs)**
723 Maximum intensity projections of confocal z-stacks of β_{PS}-Integrin, Talin and pTyr
724 immunostainings were generated in Fiji. A line spanning the MTJ and three contiguous
725 sarcomeres (as a landmark reference) was drawn with the line tool. Line intensity plots were
726 obtained with the intensity value for each pixel in the line. These values were split into five bins
727 (each bin encompassing 20% of the intensity values) along the anterior-posterior axis and an
728 average was calculated for each bin. Normalization was accomplished by calculating the deviation
729 from the mean value. We traced two lines per MTJ per larva (16-20 measurements per genotype
730 from 4-5 different larvae) and per genotype. This analysis was done in duplicate.
731
732 **Nuclear analysis**
733 All images were processed and analyzed with Fiji. 2D quantifications of VL3 and VL4 muscles
734 were performed with maximum intensity projections (as previously described in Windner et al.

735 (2019)). Muscle areas were traced by hand with the polygon tool. Automated thresholding of
736 fluorescence intensities of anti-Lamin and/or Hoechst was used to generate binary images of VL
737 nuclei. The number, size (area), position (X and Y coordinates) and shape descriptors (roundness
738 and circularity) of all nuclei within each cell was obtained and the binary masks were used to
739 quantify Hoechst and H3K9ac pixel intensity (mean gray value). Automated thresholding of anti-
740 Fibrillarin labeling was used to generate binary images of nucleoli and measure nucleolar sizes
741 (areas) and to quantify Fibrillarin pixel intensity (mean gray value). The 3D rendering of nuclei
742 was processed with Imaris.
743
744 **RNA sequencing analysis**
745 Eight to ten late third instar larvae were dissected as described above per genotype in each
746 replicate. The experiment was done in triplicate. The muscle-enriched larval filets were transferred
747 to TRIzol and homogenized. The lysates were submitted to the MSKCC's Integrated Genomics
748 Operations (IGO) core for further total RNA extraction, quality assessment and Illumina next-
749 generation sequencing. The sequencing libraries were constructed using SMARTerAmpSeq after
750 the mRNAs were enriched by oligo-dT-mediated purification. The libraries were then sequenced
751 on the Illumina HiSeq 4000 in a PE50 run. Over 40 million reads were generated per library.
752 FASTQ data was read into R with the ShortRead package (Morgan et al., 2009) and QC was
753 performed with the Rfastp package (Wang et al., 2022). Reads were mapped and aligned to the
754 *Drosophila* genome using Rsubread (Liao et al., 2019). Next, the reads were counted with the
755 GenomicAlignments package (Lawrence et al., 2013). Gene differential expression tests were
756 performed using DESeq2 (Love et al., 2014). Finally, enrichment analysis was performed through
757 goseq (Young et al., 2010) using both Gene Ontology and KEGG databases. Plots were drawn
758 using R with the ggplot2 package (Wickham, 2016).
759
760 **ATP assay**
761 An ATP calibration curve was performed using the stabilized ATP standard stocks provided in the
762 kit ATP Bioluminescence Assay Kit HS II (Millipore Sigma #11699709001) and following the
763 supplied protocol. Five to ten late third instar wandering larvae from each genotype were
764 dissected (See Immunolabeling and Imaging) and transferred into the cell lysis reagent provided
765 with the kit. Lysates were homogenized and protein concentrations were determined using the
766 Bradford assay. Equal amounts of protein (10 μg) were used for bioluminescence measurements.
767 Blank measurements were subtracted from the raw data and ATP concentrations were calculated
768 from the standard curve data. The experiment was done in triplicate.

769

770 **Statistical analysis**

771 Statistical significance was determined by either student's unpaired t-test (comparisons between
772 two groups), one-way ANOVA, or two-way ANOVA (comparisons among multiple groups) in the
773 GraphPad Prism software. Data are presented as mean±SD, asterisks are used to denote
774 significance. Graphs were made using either GraphPad Prism, Microsoft Excel or R.

775

776

ACKNOWLEDGEMENTS

We are thankful to the Baylies lab members for helpful discussions. We also thank F. Schnorrer, G. Tanentzapf, A. Beggs and V. Gupta for helpful discussions. H Bellen and F. Schöck for providing antibodies. We thank the members of the Integrated Genomics Operation (IGO) and the Bioinformatics Cores at MSKCC.

AUTHOR CONTRIBUTIONS

Conceptualization: C.Z.M. and M.K.B; Methodology: C.Z.M., P.J.C, D.S.; Validation: C.Z.M. P.J.C, D.S; Formal analysis: C.Z.M., P.J.C, D.S.; Investigation: C.Z.M., P.J.C, D.S.; Resources: R.D., M.K.B.; Data curation: C.Z.M., M.K.B.; Writing - original draft: C.Z.M., M.K.B.; Writing - review & editing: C.Z.M., P.J.C., R.D., S.E.W., M.K.B.; Visualization: C.Z.M.; Supervision: R.D., M.K.B.; Project administration: C.Z.M., P.J.C., M.K.B.; Funding acquisition: M.K.B., R.D., P.J.C.

COMPETING INTERESTS

The authors declare no competing interests.

FUNDING

This work was supported by National Institutes of Health grants R01 AR068128 and R35 GM141877 to M.K.B.; National Institutes of Health grant R01 GM073791 to R.D. and a Blavatnik Family Foundation predoctoral fellowship to P.J.C.

DATA AVAILABILITY

RNA-seq data have been deposited in Gene Expression Omnibus (GEO) under the accession number GSE210507.

803 **FIGURES**

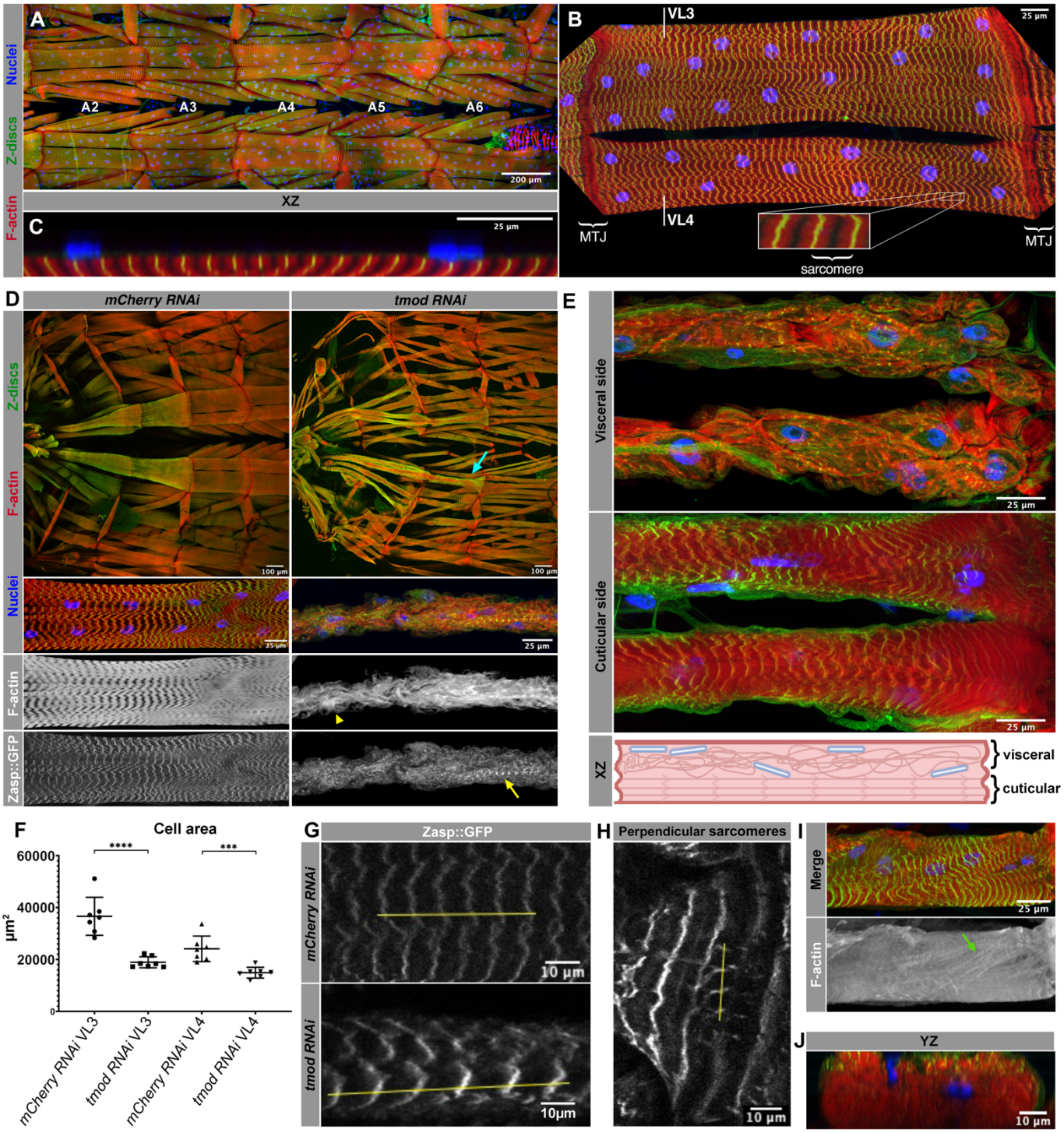

804

805 **Fig. 1: Tmod is required for larval muscle integrity.**

806 (A) Third instar *Drosophila* larval filet displaying abdominal segments (A2-6) and body wall
807 muscles (red, phalloidin) with Z-discs (green, Zasp::GFP) and nuclei (blue, Hoechst); anterior,
808 left.
809 (B) Z-stack projection of VL3 and VL4 muscles showing MTJs and zoomed-in panel of a
810 sarcomere.
811 (C) Longitudinal cross-section of a VL4 myofiber with nuclei on the cell surface.
812 (D) Overview of anterior musculature in control and Tmod KD larvae (top). Higher magnification
813 of VL3 muscle merge, F-actin and Zasp::GFP (bottom 3 panels). Cyan arrow indicates width
814 reduction of the myofiber. Yellow arrowhead indicates ectopic F-actin. Yellow arrow indicates a
815 remaining myofibril.
816 (E) Visceral view of VL3 and VL4 Tmod KD muscles showing disorganized myofibrils and ectopic
817 F-actin (top), cuticular view showing conserved sarcomeres (middle) and cross-sectional diagram
818 showing how both visceral and cuticular sides are integrated in a myofiber (bottom).
819 (F) Average VL3 and VL4 myofiber areas in control and *tmod* KD larvae from A2 in wandering
820 late third instars. Graph represents one experiment (N>3 replicates, each with n_{VL3}=7 myofibers
821 and n_{VL4}=7 myofibers per genotype; p_{VL3}<0.0001 and p_{VL4}=0.0006, two-tailed unpaired Student's
822 t-test). Error bars show SD.
823 (G) Sarcomere length in control and *tmod* KD myofibers. Yellow line spans six Z-discs.
824 (H) Perpendicular sarcomeres observed in *tmod* KD myofibers. Yellow line spans 4 Z-discs.
825 (I) Disorganized and misoriented myofibrils. Green arrow indicates diagonally oriented myofibrils.
826 (J) Optical cross-section of *tmod* KD myofiber displaying internalized and misshapen nuclei.
827 Scale bars: 200μm (A), 100μm (top panels in D), 25μm (B, C, bottom 3 panels in D, E and I) and
828 10μm (G, H and J).

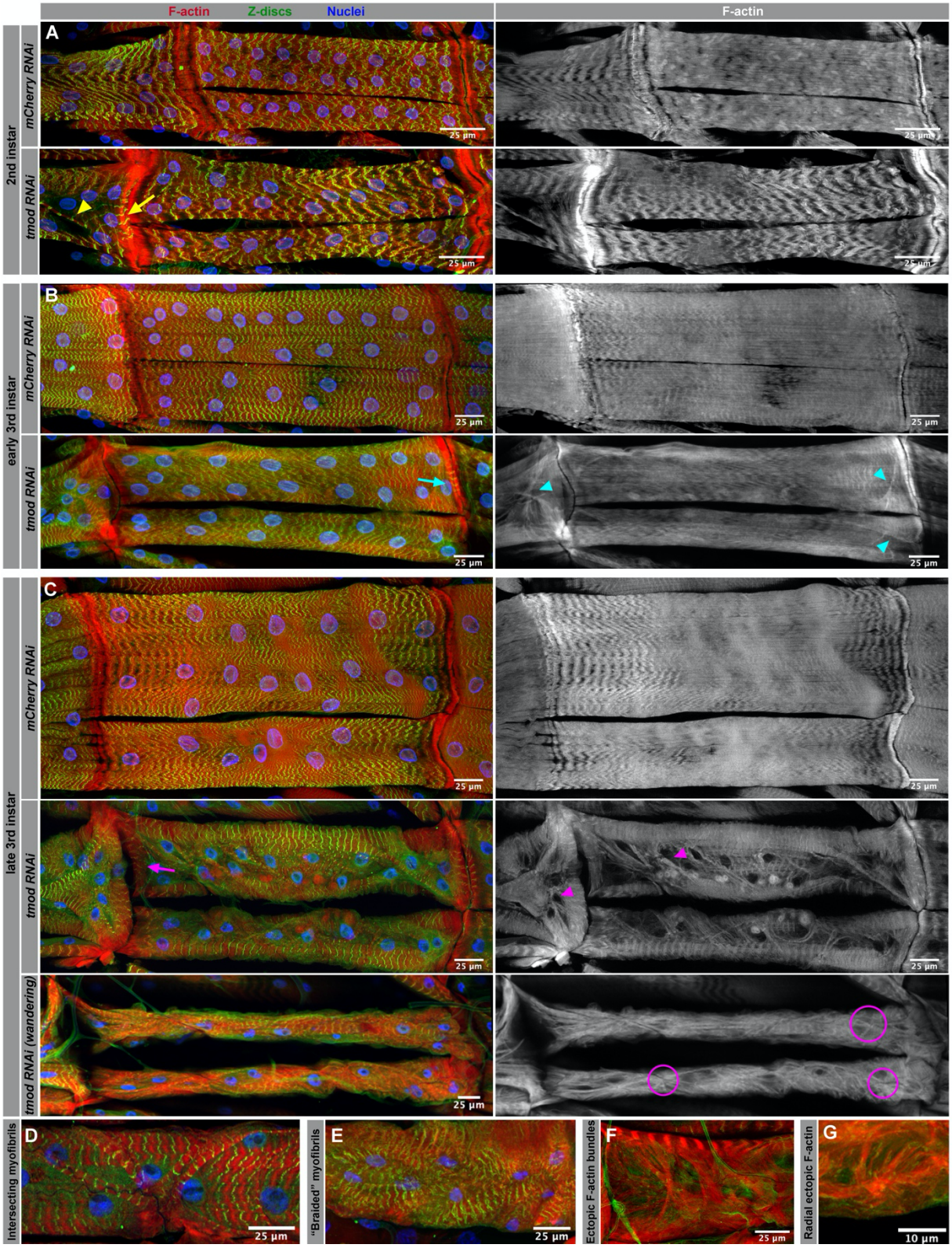
F-actin
Z-discs
Nuclei
F-actin
A
B
C
D
E
F
G
2nd instar
early 3rd instar
late 3rd instar
mCherry RNAi
tmod RNAi
tmod RNAi (wandering)
Intersecting myofibrils
"Braided" myofibrils
Ectopic F-actin bundles
Radial ectopic F-actin
25 µm
10 µm

829

830 **Fig. 2: Structural patterned deterioration of *tmod* KD myofibers throughout the *Drosophila***
831 **larval stages.**
832 (A) Posterior end of VI1 myofiber from A1 segment and full length VL3 and VL4 myofibers from
833 A2 segment in control and *tmod* KD second instar larvae (red, phalloidin; green, Zasp::GFP and
834 blue, Hoechst) (left). F-actin channel only (gray, phalloidin) (right). Yellow arrowhead indicates
835 diagonally misoriented myofibril in VI1 from A1. Yellow arrow indicates perpendicular misoriented
836 myofibrils in VI1 from A1.
837 (B) Worsening myofibers from A1 and A2 segment in *tmod* KD early third instars (bottom) when
838 compared to controls (top). Cyan arrowheads indicate diagonally misoriented myofibrils. Cyan
839 arrow indicates perpendicular myofibrils in posterior end of VL3 muscle from A2.
840 (C) Worsening myofibers from A1 and A2 in *tmod* KD late third instars (middle panels) and
841 wandering late third instar (bottom panel) when compared to control (top panel). Magenta
842 arrowheads indicate worsening of diagonally misoriented myofibrils from A1 and A2. Magenta
843 arrow indicates perpendicular myofibrils in anterior end of VL3 muscle from A2. Magenta circles
844 indicate ectopic F-actin structures that replace stereotypical myofibrillar pattern. Quantifications
845 of the defects observed in panels A, B, and C across the A-P axis in Supplemental Fig2D.
846 (D) Intersecting grouped myofibrils observed during early third instar.
847 (E) Interlaced or “braided” myofibrils observed during late third instar.
848 (F and G) Ectopic F-actin bundles and radial actin structures, respectively, that lack myofibrillar
849 pattern observed during wandering late third instar.
850 N=3 replicates, each with n=5 larvae per stage
851 Scale bars: 25μm (A-F) and 10μm (G).
852

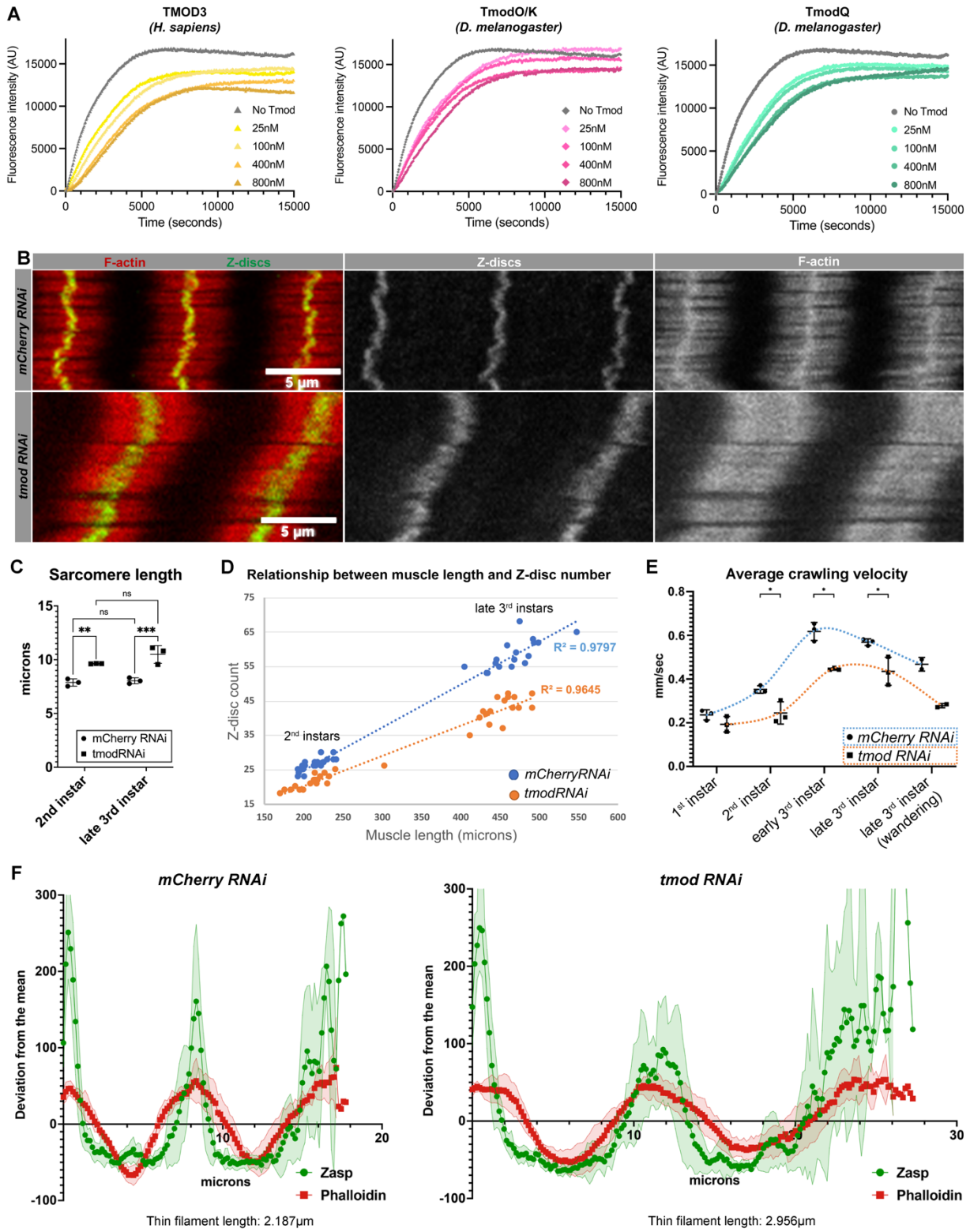

Fig. 3: *Drosophila* Tmod is a capping protein and *tmod* KD myofibers display longer thin filaments and sarcomeres.

856 (A) Pyrene-labeled actin polymerization assays at the pointed end with human TMOD3,
857 *Drosophila* TmodO/K and *Drosophila* TmodQ at multiple concentrations (n=4, per isoform and per
858 concentration).
859 (B) Sarcomeres from control myofibers and from *tmod* KD myofibers found at the cuticular side
860 of late third instars in A2 (red, phalloidin and green, Zasp) (left). Middle panel shows Zasp channel
861 and right panel shows phalloidin channel.
862 (C) Average sarcomere length in control and *tmod* KD VL3 myofibers from A2 in second instars
863 and late third instars. Each dot is one experiment (N=3 replicates with $n_{2nd\ instars}$=75-135, $n_{late\ 3rd}$
864 $_{instars}$=45-105 sarcomeres [from 3-8 different larvae] per genotype and per experiment; p_{2nd}
865 $_{instars}$=0.0076, $p_{3rd\ instars}$=0.0009, $p_{mCherryRNAi}$=0.9703, $p_{tmodRNAi}$=0.1843, ordinary 2-way ANOVA
866 multiple comparisons). Error bars show SD.
867 (D) Scatterplots and regression lines (dotted) comparing Z-disc number in relationship to muscle
868 length (in microns) in control (blue) and *tmod* KD (orange) VL3 myofibers from A2 in second
869 instars and late third instars. R^2 are indicated in the plot. N=3 experiments, with $n_{2nd\ instars}$=19-20,
870 $n_{late\ 3rd\ instars}$=16-17 myofibers per genotype.
871 (E) Average crawling velocities from each larval stage in control (blue) and *tmod* KD (orange).
872 Each dot is one experiment (N=3 replicates, with $n_{1st\ instars}$=10, $n_{2nd\ instars}$=10, $n_{early\ 3rd\ instars}$=5-10, n_{late}
873 $_{3rd\ instars}$= 3-10, $n_{wandering}$=3-4 larvae per genotype and per experiment; $p_{1st\ instars}$=0.245, p_{2nd}
874 $_{instars}$=0.0326, $p_{early\ 3rd\ instars}$=0.0182, $p_{late\ 3rd\ instars}$=0.0433, $p_{wandering}$=0.0507, two-tailed paired
875 Student's t-test). Error bars show SD.
876 (F) Fluorescent intensities of phalloidin (red) and Zasp::GFP (green) normalized as the deviation
877 from the mean and plotted across the length of two sarcomeres in A2 of late third instars. Thin
878 filament length is obtained from the length under the center peak divided in half (n=4-6 muscles
879 from different larva per genotype). Transparent zones show SD.
880 Scale bars: 5μm (B).
881
882
883
884
885
886
887
888
889

890
891
892
893

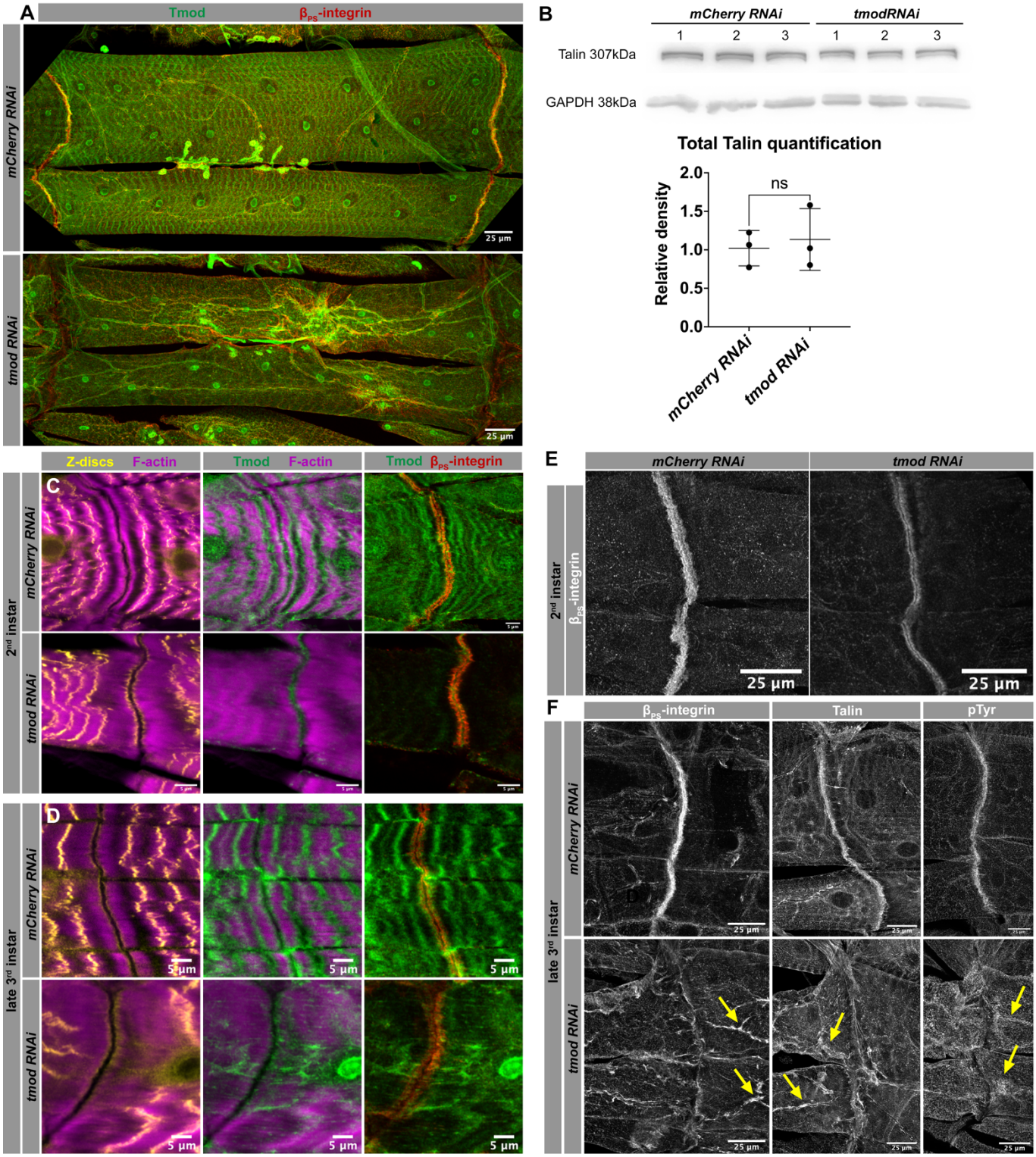

Fig. 4: Tmod KD muscles exhibit a decrease in Tmod and loss of mechanosensory protein enrichment and tension at the MTJ.

(A) VL3 and VL4 myofibers in A2 from late third instars in control and *tmod* KD larvae. In control myofibers, Tmod (green) displays a stereotypical pattern in the sarcomeres and its colocalization

898 with β_{PS}-integrin (red) at the MTJ (top panel). In *tmod* KD myofibers, Tmod does not appear to be
899 present at the same intensity levels on the sarcomeres nor at the MTJ (bottom panel).
900 (B) Western blot and quantification of Talin in late third instar muscle-enriched lysates.
901 Glyceraldehyde 3-phosphate dehydrogenase (GAPDH) as loading control. Each dot is an
902 experiment (N=3 replicates, with n=5-10 larval carcasses per genotype and per experiment,
903 p=0.7846, two-tailed paired Student's t-test). Error bars show SD.
904 (C and D) Analysis of protein localization (magenta, phalloidin; yellow, Zasp::GFP; green, Tmod;
905 and red, β_{PS}-integrin) relative to one another at the MTJ (A2-3) in control and *tmod* KD in second
906 and late third instar larvae.
907 (E) β_{PS}-integrin (white) strong enrichment at the MTJ (A2-3) in second instar control larvae
908 compared to decreased signal in *tmod* KD. Quantification in Supplemental Fig 5A.
909 (F) β_{PS}-integrin (left), Talin (white, middle) and pTyr (white, right) strong enrichment at the MTJ
910 (A2-3) in wandering third instar control larvae compared to absence of signal in *tmod* KD.
911 Quantifications in Supplemental Fig 5B. Yellow arrows indicate ectopic pools of protein.
912 Scale bars: 5μm (C, D) and 25μm (A, E, and F).
913

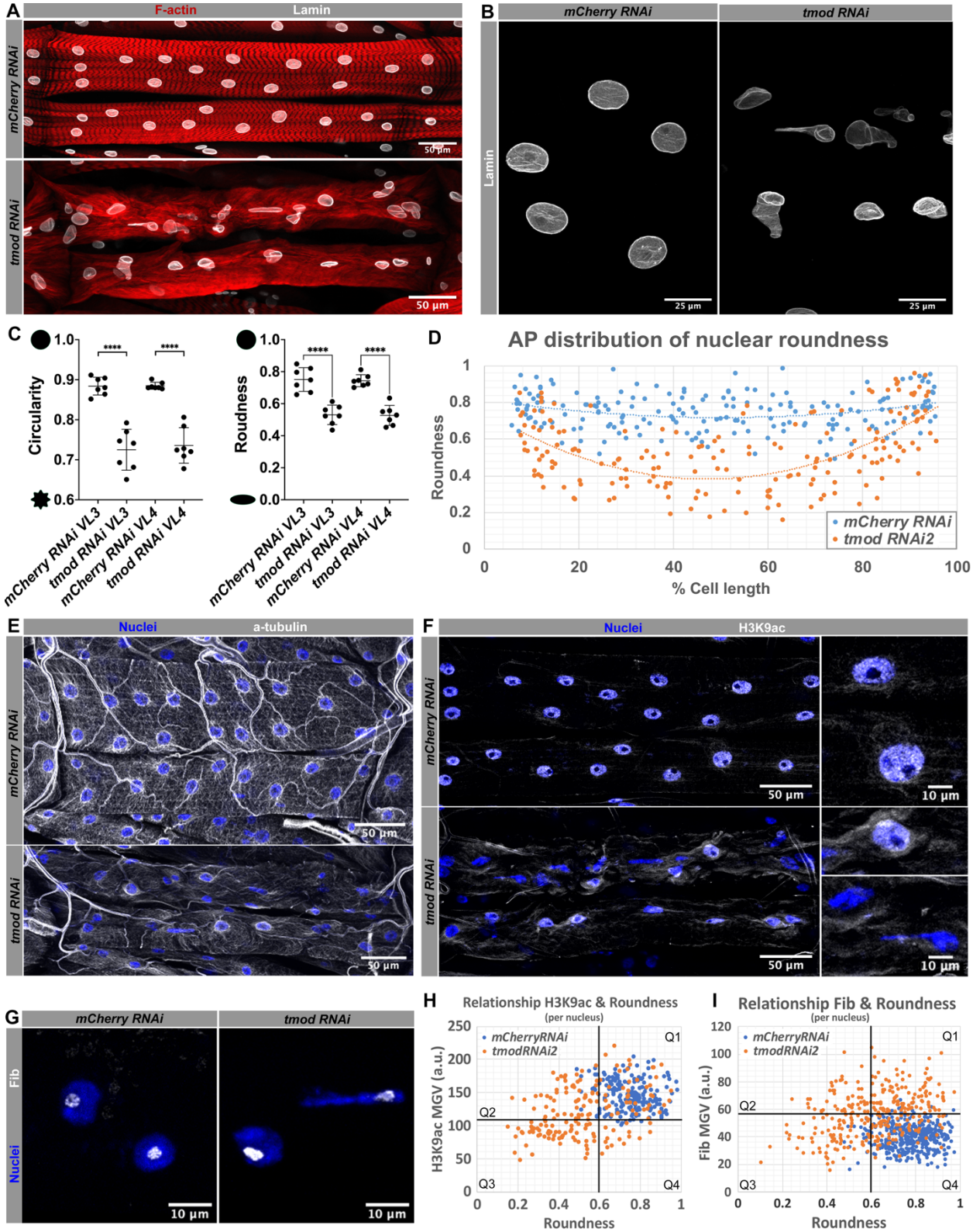

Fig. 5: Tmod KD myofibers display misshapen and dysfunctional nuclei in late third instars.

917 (A) VL3 and VL4 myofibers (red, phalloidin) with nuclei (white, Lamin) in A2 in control (top) and
918 *tmod* KD larvae (bottom).
919 (B) High magnification panels of myonuclei (white, Lamin) with control nuclei and misshapen and
920 internalized *tmod* KD nuclei. See supplemental Movie 1 and 2.
921 (C) Quantification of two shape descriptors: average circularity and average roundness in VL3
922 and VL4 myofibers in A2 from control and *tmod* KD. Graph represents one experiment, each dot
923 is one myofiber per larva (n_{VL3}= 15-20, n_{VL4}=8-11 myonuclei per myofiber and per genotype;
924 circularity p_{VL3}<0.0001, circularity p_{VL4}<0.0001; roundness p_{VL3}<0.0001, roundness p_{VL4}<0.0001,
925 ordinary one-way ANOVA multiple comparisons). Experiment repeated N>3. Error bars show SD.
926 (D) Distribution of nuclear roundness along the AP axis of the myofiber from control (blue) and
927 *tmod* KD (orange) myofibers. Polynomial trendline shown by curved dotted lines.
928 (E) MT staining (white, α-tubulin; blue, nuclei) showing radial perinuclear arrays and longitudinal
929 tracks in the control myofibers and a decrease of these structures in *tmod* KD.
930 (F-G) H3K9ac and Fib staining (white) indicating sites of active transcription and translation
931 respectively in myonuclei both in control and *tmod* KD myofibers.
932 (H and I) Scatterplots showing H3K9ac and Fib pixel intensity levels (mean gray value) in
933 relationship to roundness levels. Each graph represents one experiment, each dot is one
934 myonucleus (n_{H3K9ac}=178-190 myonuclei per genotype, from 7 VL3 and VL4 muscles sets, in 7
935 larvae; n_{Fib}=308-396 myonuclei per genotype, from 12-15 VL3 and VL4 muscle sets, in 7-8
936 larvae). (H) Q3 indicates *tmod* KD misshaped nuclei (roundness<0.6) with decreased H3K9ac
937 intensity when compared to control nuclei in Q1. (I) Q1 indicates *tmod* KD WT-like nuclei
938 (roundness>0.6) with increased Fib intensity when compared to control nuclei in Q4. Q3 indicate
939 *tmod* KD misshaped nuclei (roundness<0.6) with a similar Fib intensity when compared to control
940 nuclei.
941 Experiments repeated N>2 unless specified otherwise.
942 Scale bars: 50μm (A, E and F), 25μm (B) and 10μm (F and G).
943

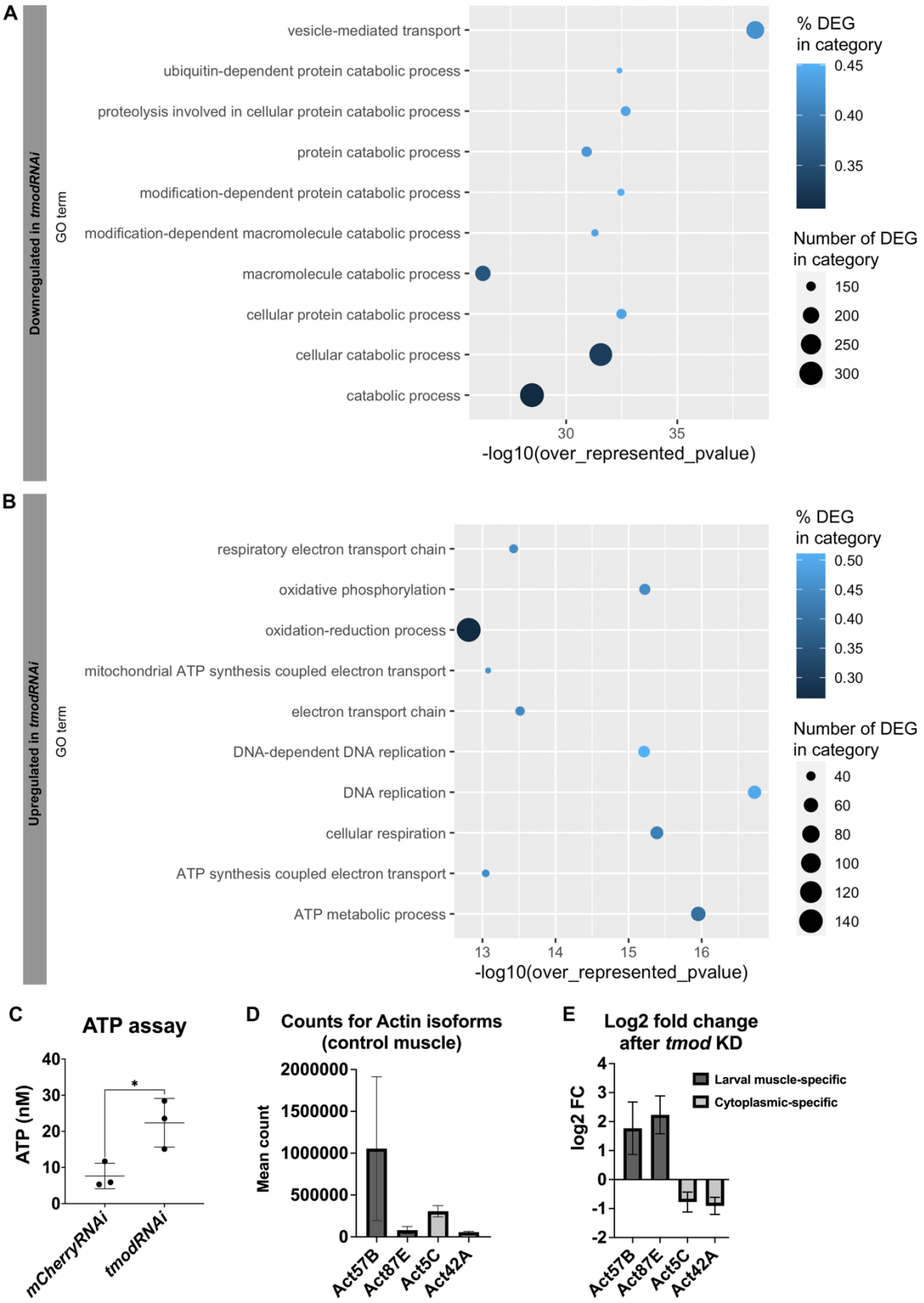

Fig. 6: Tmod KD late third instar larvae show differential gene expression (DEG) when compared to control.

947 (A and B) Top 10 downregulated and upregulated Gene Ontology gene sets in *tmod* KD vs control
948 larvae assessed by ORA.
949 (C) Average ATP concentration in muscle-enriched larval lysates. Each dot is one experiment
950 (N=3 replicates, n=5-10 larval carcasses per genotype and per experiment, p=0.0285, two-tailed
951 unpaired Student's t-test). Error bars show SD.
952 (D) Normalized counts average for the different *Drosophila* actin genes in control larvae. Error
953 bars show SD.
954 (E) Log2 fold change of actin genes isoforms in *tmod* KD vs control (p_{Act57B}=0.0053,
955 p_{Act87E}<0.0001, p_{Act5E}= 0.0011, p_{Act42A}<0.0001). Error bars show SE. RNAseq data was used for
956 plots A, B, D and E (N=3 replicates, n=7-10 larval carcasses per genotype and per N).
957

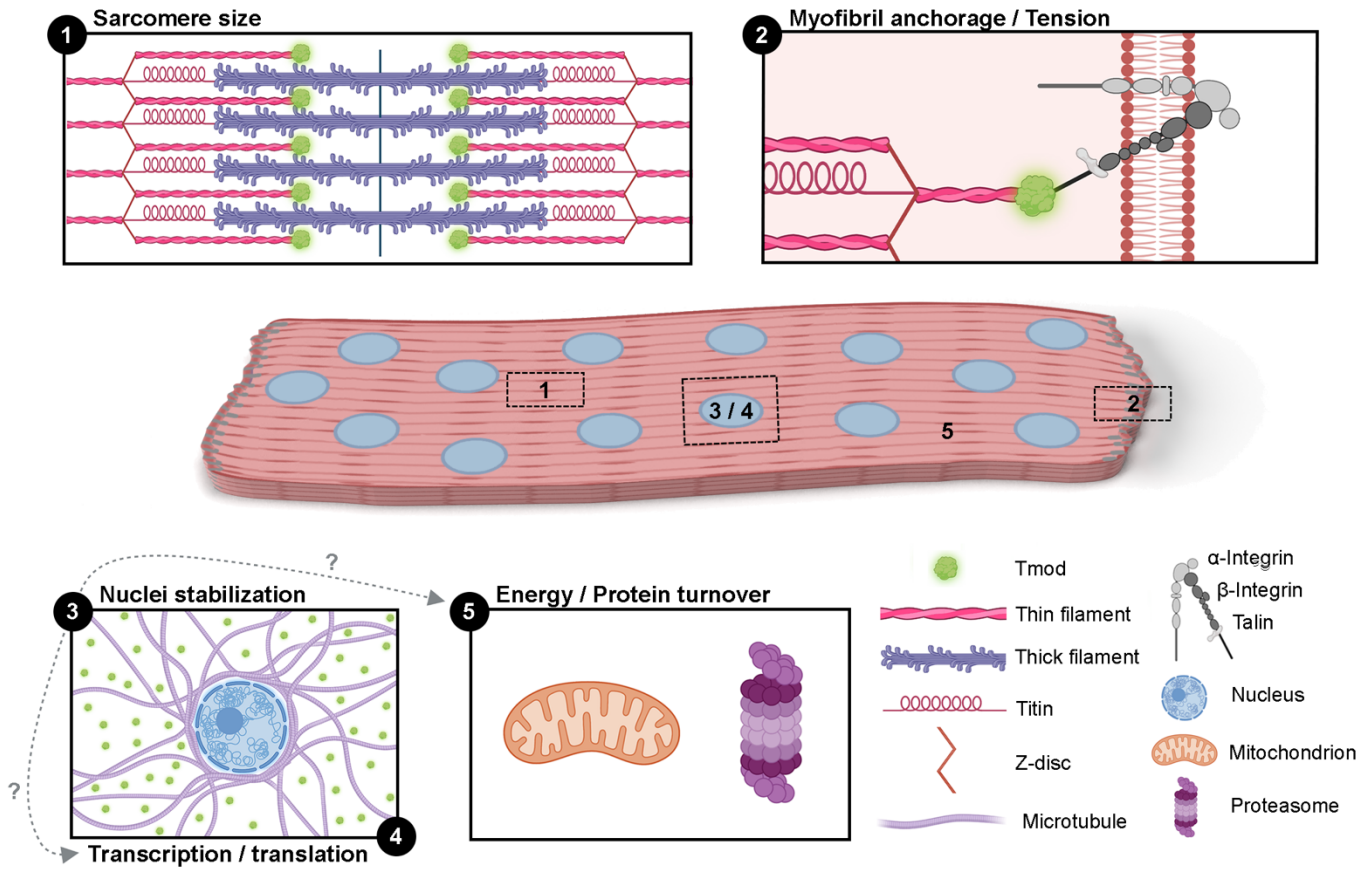

Fig. 7: Summary of the diverse roles of Tmod in *Drosophila* larva myofibers.
(1) Sarcomere size: Tmod plays a role in sarcomere and thin filament length.
(2) Myofibril anchorage: Tmod stabilizes the interaction of β_{PS}-integrin/Talin at the MTJ, and is found adjacent to F-actin, suggesting a role establishing tension in the longitudinal axis of the myofiber.
(3) Nuclear stabilization: Tmod plays a role in maintaining nuclear integrity either through MT-actin interactions or through nuclear F-actin.
(4) Transcription / translation: Tmod is important for normal nuclear output. Potentially through actin as a transcription factor in the nucleus or as a structural component, or by actin's role in nuclear architecture and chromatin organization that would impact transcription/translation.
(5) Energy / Protein turnover: Upon Tmod KD, we observed an increase in energy production (ATP) genes and a decrease of proteasome genes. This change in transcriptome could be due to the role of Tmod in nuclear stabilization or as an attempt of the myofiber to keep growing.
Grey dashed arrows and question marks indicate potential consequences.

974 **REFERENCES**

975

976 ATHERTON, P., STUTCHBURY, B., JETHWA, D. & BALLESTREM, C. 2016.
977 Mechanosensitive components of integrin adhesions: Role of vinculin. *Exp Cell Res,* 343**,**
978 21-27.

979 AVELLANEDA, J., RODIER, C., DAIAN, F., BROUILLY, N., RIVAL, T., LUIS, N. M. &
980 SCHNORRER, F. 2021. Myofibril and mitochondria morphogenesis are coordinated by a
981 mechanical feedback mechanism in muscle. *Nat Commun,* 12**,** 2091.

982 BAI, J., HARTWIG, J. H. & PERRIMON, N. 2007. SALS, a WH2-domain-containing protein,
983 promotes sarcomeric actin filament elongation from pointed ends during Drosophila
984 muscle growth. *Dev Cell,* 13**,** 828-42.

985 BALAKRISHNAN, M., SISSO, W. J. & BAYLIES, M. K. 2021. Analyzing muscle structure and
986 function throughout the larval instars in live Drosophila. *STAR Protoc,* 2**,** 100291.

987 BALAKRISHNAN, M., YU, S. F., CHIN, S. M., SOFFAR, D. B., WINDNER, S. E., GOODE, B.
988 L. & BAYLIES, M. K. 2020. Cofilin Loss in Drosophila Muscles Contributes to Muscle
989 Weakness through Defective Sarcomerogenesis during Muscle Growth. *Cell Rep,* 32**,**
990 107893.

991 BAROHN, R. J., DIMACHKIE, M. M. & JACKSON, C. E. 2014. A pattern recognition approach
992 to patients with a suspected myopathy. *Neurol Clin,* 32**,** 569-93, vii.

993 BATE, M. 1990. The embryonic development of larval muscles in Drosophila. *Development,*
994 110**,** 791-804.

995 BAWA, S., BROOKS, D. S., NEVILLE, K. E., TIPPING, M., SAGAR, M. A., KOLLHOFF, J. A.,
996 CHAWLA, G., GEISBRECHT, B. V., TENNESSEN, J. M., ELICEIRI, K. W. &
997 GEISBRECHT, E. R. 2020. Drosophila TRIM32 cooperates with glycolytic enzymes to
998 promote cell growth. *Elife,* 9.

999 BECKER, R., LEONE, M. & ENGEL, F. B. 2020. Microtubule Organization in Striated Muscle
1000 Cells. *Cells,* 9.

1001 BERGER, J., BERGER, S., MOK, Y. S. G., LI, M., TARAKCI, H. & CURRIE, P. D. 2022.
1002 Genetic dissection of novel myopathy models reveals a role of CapZalpha and Leiomodin
1003 3 during myofibril elongation. *PLoS Genet,* 18**,** e1010066.

1004 BERGER, J., TARAKCI, H., BERGER, S., LI, M., HALL, T. E., ARNER, A. & CURRIE, P. D.
1005 2014. Loss of Tropomodulin4 in the zebrafish mutant trage causes cytoplasmic rod
1006 formation and muscle weakness reminiscent of nemaline myopathy. *Dis Model Mech,* 7**,**
1007 1407-15.

1008 BETTINGER, B. T., GILBERT, D. M. & AMBERG, D. C. 2004. Actin up in the nucleus. *Nat Rev*
1009 *Mol Cell Biol,* 5**,** 410-5.
1010 BODENSTEIN, D. 1950. The Postembryonic Development of Drosophila. *In:* M, D. (ed.)
1011 *Biology of Drosophila.* Cold Spring Harbor Laboratory Press.
1012 BONNEMANN, C. G. & LAING, N. G. 2004. Myopathies resulting from mutations in sarcomeric
1013 proteins. *Curr Opin Neurol,* 17**,** 529-37.
1014 BRAND, A. H. & PERRIMON, N. 1993. Targeted gene expression as a means of altering cell
1015 fates and generating dominant phenotypes. *Development,* 118**,** 401-15.
1016 BRENT, J. R., WERNER, K. M. & MCCABE, B. D. 2009. Drosophila larval NMJ dissection. *J*
1017 *Vis Exp*.
1018 BROOKS, D., BAWA, S., BONTRAGER, A., STETSIV, M., GUO, Y. & GEISBRECHT, E. R.
1019 2022. Independent pathways control muscle tissue size and sarcomere remodeling. *Dev*
1020 *Biol,* 490**,** 1-12.
1021 CARIDI, C. P., PLESSNER, M., GROSSE, R. & CHIOLO, I. 2019. Nuclear actin filaments in
1022 DNA repair dynamics. *Nat Cell Biol,* 21**,** 1068-1077.
1023 CASSANDRINI, D., TROVATO, R., RUBEGNI, A., LENZI, S., FIORILLO, C., BALDACCI, J.,
1024 MINETTI, C., ASTREA, G., BRUNO, C., SANTORELLI, F. M. & ITALIAN NETWORK ON
1025 CONGENITAL, M. 2017. Congenital myopathies: clinical phenotypes and new diagnostic
1026 tools. *Ital J Pediatr,* 43**,** 101.
1027 CENIK, B. K., GARG, A., MCANALLY, J. R., SHELTON, J. M., RICHARDSON, J. A., BASSEL-
1028 DUBY, R., OLSON, E. N. & LIU, N. 2015. Severe myopathy in mice lacking the
1029 MEF2/SRF-dependent gene leiomodin-3. *J Clin Invest,* 125**,** 1569-78.
1030 CHANG, W., ANTOKU, S., OSTLUND, C., WORMAN, H. J. & GUNDERSEN, G. G. 2015.
1031 Linker of nucleoskeleton and cytoskeleton (LINC) complex-mediated actin-dependent
1032 nuclear positioning orients centrosomes in migrating myoblasts. *Nucleus,* 6**,** 77-88.
1033 CHARVET, B., RUGGIERO, F. & LE GUELLEC, D. 2012. The development of the
1034 myotendinous junction. A review. *Muscles Ligaments Tendons J,* 2**,** 53-63.
1035 CHASE, P. B., SZCZYPINSKI, M. P. & SOTO, E. P. 2013. Nuclear tropomyosin and troponin
1036 in striated muscle: new roles in a new locale? *J Muscle Res Cell Motil,* 34**,** 275-84.
1037 CHEREAU, D., BOCZKOWSKA, M., SKWAREK-MARUSZEWSKA, A., FUJIWARA, I.,
1038 HAYES, D. B., REBOWSKI, G., LAPPALAINEN, P., POLLARD, T. D. & DOMINGUEZ, R.
1039 2008. Leiomodin is an actin filament nucleator in muscle cells. *Science,* 320**,** 239-43.

1040 CHRISTOPHERS, B., LOPEZ, M. A., GUPTA, V. A., VOGEL, H. & BAYLIES, M. 2022.
1041 Pediatric Nemaline Myopathy: A Systematic Review Using Individual Patient Data. *Journal*
1042 *of Child Neurology,* 37**,** 652-663.
1043 CHRZANOWSKA-WODNICKA, M. & BURRIDGE, K. 1994. Tyrosine phosphorylation is
1044 involved in reorganization of the actin cytoskeleton in response to serum or LPA
1045 stimulation. *J Cell Sci,* 107 (Pt 12)**,** 3643-54.
1046 DAVIDSON, P. M. & CADOT, B. 2021. Actin on and around the Nucleus. *Trends Cell Biol,* 31**,**
1047 211-223.
1048 DE WINTER, J. M. & OTTENHEIJM, C. A. C. 2017. Sarcomere Dysfunction in Nemaline
1049 Myopathy. *J Neuromuscul Dis,* 4**,** 99-113.
1050 DEMONTIS, F. & PERRIMON, N. 2009. Integration of Insulin receptor/Foxo signaling and
1051 dMyc activity during muscle growth regulates body size in Drosophila. *Development,* 136**,**
1052 983-93.
1053 DENG, S., SILIMON, R. L., BALAKRISHNAN, M., BOTHE, I., JUROS, D., SOFFAR, D. B. &
1054 BAYLIES, M. K. 2021. The actin polymerization factor Diaphanous and the actin severing
1055 protein Flightless I collaborate to regulate sarcomere size. *Dev Biol,* 469**,** 12-25.
1056 DIX, D. J. & EISENBERG, B. R. 1990. Myosin mRNA accumulation and myofibrillogenesis at
1057 the myotendinous junction of stretched muscle fibers. *J Cell Biol,* 111**,** 1885-94.
1058 DLUGOSZ, A. A., ANTIN, P. B., NACHMIAS, V. T. & HOLTZER, H. 1984. The relationship
1059 between stress fiber-like structures and nascent myofibrils in cultured cardiac myocytes.
1060 *J Cell Biol,* 99**,** 2268-78.
1061 DOGTEROM, M. & KOENDERINK, G. H. 2019. Actin-microtubule crosstalk in cell biology. *Nat*
1062 *Rev Mol Cell Biol,* 20**,** 38-54.
1063 DOOLITTLE, L. K., ROSEN, M. K. & PADRICK, S. B. 2013. Measurement and analysis of in
1064 vitro actin polymerization. *Methods Mol Biol,* 1046**,** 273-93.
1065 DYE, C. A., LEE, J. K., ATKINSON, R. C., BREWSTER, R., HAN, P. L. & BELLEN, H. J. 1998.
1066 The Drosophila sanpodo gene controls sibling cell fate and encodes a tropomodulin
1067 homolog, an actin/tropomyosin-associated protein. *Development,* 125**,** 1845-56.
1068 FARINA, F., GAILLARD, J., GUERIN, C., COUTE, Y., SILLIBOURNE, J., BLANCHOIN, L. &
1069 THERY, M. 2016. The centrosome is an actin-organizing centre. *Nat Cell Biol,* 18**,** 65-75.
1070 FENG, Y., UEDA, A. & WU, C. F. 2004. A modified minimal hemolymph-like solution, HL3.1,
1071 for physiological recordings at the neuromuscular junctions of normal and mutant
1072 Drosophila larvae. *J Neurogenet,* 18**,** 377-402.

1073 FENIX, A. M., NEININGER, A. C., TANEJA, N., HYDE, K., VISETSOUK, M. R., GARDE, R.
1074 J., LIU, B., NIXON, B. R., MANALO, A. E., BECKER, J. R., CRAWLEY, S. W., BADER,
1075 D. M., TYSKA, M. J., LIU, Q., GUTZMAN, J. H. & BURNETTE, D. T. 2018. Muscle-specific
1076 stress fibers give rise to sarcomeres in cardiomyocytes. *Elife,* 7.
1077 FERNANDES, I. & SCHOCK, F. 2014. The nebulin repeat protein Lasp regulates I-band
1078 architecture and filament spacing in myofibrils. *J Cell Biol,* 206**,** 559-72.
1079 FISCHER, R. S., YARMOLA, E. G., WEBER, K. L., SPEICHER, K. D., SPEICHER, D. W.,
1080 BUBB, M. R. & FOWLER, V. M. 2006. Tropomodulin 3 binds to actin monomers. *J Biol*
1081 *Chem,* 281**,** 36454-65.
1082 FOWLER, V. M. 1997. Capping actin filament growth: tropomodulin in muscle and nonmuscle
1083 cells. *Soc Gen Physiol Ser,* 52**,** 79-89.
1084 FOWLER, V. M. & DOMINGUEZ, R. 2017. Tropomodulins and Leiomodins: Actin Pointed End
1085 Caps and Nucleators in Muscles. *Biophys J,* 112**,** 1742-1760.
1086 FYRBERG, E. A., MAHAFFEY, J. W., BOND, B. J. & DAVIDSON, N. 1983. Transcripts of the
1087 six Drosophila actin genes accumulate in a stage- and tissue-specific manner. *Cell,* 33**,**
1088 115-23.
1089 GHOSH, A. & FOWLER, V. M. 2021. Tropomodulins. *Curr Biol,* 31**,** R501-R503.
1090 GILLERY, P., GEORGES, N., RANDOUX, A., LEFEVRE, F., MAQUART, F. X. & BOREL, J.
1091 P. 1996. Modulation of protein synthesis by extracellular matrix: potential involvement of
1092 two nucleolar proteins, nucleolin and fibrillarin. *Biochem Biophys Res Commun,* 228**,** 94-
1093 9.
1094 GOKHIN, D. S. & FOWLER, V. M. 2013. A two-segment model for thin filament architecture in
1095 skeletal muscle. *Nat Rev Mol Cell Biol,* 14**,** 113-9.
1096 GOLDSPINK, G. 1983. Alterations in Myofibril Size and Structure During Growth, Exercise,
1097 and Changes in Environmental Temperature. *Comprehensive Physiology.*
1098 GREGORIO, C. C., WEBER, A., BONDAD, M., PENNISE, C. R. & FOWLER, V. M. 1995.
1099 Requirement of pointed-end capping by tropomodulin to maintain actin filament length in
1100 embryonic chick cardiac myocytes. *Nature,* 377**,** 83-6.
1101 HAAS, J. N. 1950. Cytoplasmic growth in the muscle fibers of larvae of Drosophila
1102 melanogaster. *Growth,* 14**,** 277-94.
1103 KEE, A. J., GUNNING, P. W. & HARDEMAN, E. C. 2009. Diverse roles of the actin
1104 cytoskeleton in striated muscle. *J Muscle Res Cell Motil,* 30**,** 187-97.
1105 KUMARI, R., JIU, Y., CARMAN, P. J., TOJKANDER, S., KOGAN, K., VARJOSALO, M.,
1106 GUNNING, P. W., DOMINGUEZ, R. & LAPPALAINEN, P. 2020. Tropomodulins Control

1107 the Balance between Protrusive and Contractile Structures by Stabilizing Actin-
1108 Tropomyosin Filaments. *Curr Biol,* 30**,** 767-778 e5.
1109 LABEAU-DIMENNA, E. M., CLARK, K. A., BAUMAN, K. D., PARKER, D. S., CRIPPS, R. M.
1110 & GEISBRECHT, E. R. 2012. Thin, a Trim32 ortholog, is essential for myofibril stability
1111 and is required for the integrity of the costamere in Drosophila. *Proc Natl Acad Sci U S A,*
1112 109**,** 17983-8.
1113 LAHIRI, S., SHEN, K., KLEIN, M., TANG, A., KANE, E., GERSHOW, M., GARRITY, P. &
1114 SAMUEL, A. D. 2011. Two alternating motor programs drive navigation in Drosophila
1115 larva. *PLoS One,* 6**,** e23180.
1116 LAITILA, J. & WALLGREN-PETTERSSON, C. 2021. Recent advances in nemaline myopathy.
1117 *Neuromuscul Disord,* 31**,** 955-967.
1118 LAWRENCE, M., HUBER, W., PAGES, H., ABOYOUN, P., CARLSON, M., GENTLEMAN, R.,
1119 MORGAN, M. T. & CAREY, V. J. 2013. Software for computing and annotating genomic
1120 ranges. *PLoS Comput Biol,* 9**,** e1003118.
1121 LEE, H. S., LIM, C. J., PUZON-MCLAUGHLIN, W., SHATTIL, S. J. & GINSBERG, M. H. 2009.
1122 RIAM activates integrins by linking talin to ras GTPase membrane-targeting sequences. *J*
1123 *Biol Chem,* 284**,** 5119-27.
1124 LEFEVRE, F., GARNOTEL, R., GEORGES, N. & GILLERY, P. 2001. Modulation of collagen
1125 metabolism by the nucleolar protein fibrillarin. *Exp Cell Res,* 271**,** 84-93.
1126 LEGOFF, L. & LECUIT, T. 2015. Mechanical Forces and Growth in Animal Tissues. *Cold*
1127 *Spring Harb Perspect Biol,* 8**,** a019232.
1128 LEMKE, S. B. & SCHNORRER, F. 2017. Mechanical forces during muscle development. *Mech*
1129 *Dev,* 144**,** 92-101.
1130 LEMKE, S. B., WEIDEMANN, T., COST, A. L., GRASHOFF, C. & SCHNORRER, F. 2019. A
1131 small proportion of Talin molecules transmit forces at developing muscle attachments in
1132 vivo. *PLoS Biol,* 17**,** e3000057.
1133 LIAO, Y., SMYTH, G. K. & SHI, W. 2019. The R package Rsubread is easier, faster, cheaper
1134 and better for alignment and quantification of RNA sequencing reads. *Nucleic Acids Res,*
1135 47**,** e47.
1136 LITTLEFIELD, R., ALMENAR-QUERALT, A. & FOWLER, V. M. 2001. Actin dynamics at
1137 pointed ends regulates thin filament length in striated muscle. *Nat Cell Biol,* 3**,** 544-51.
1138 LITTLEFIELD, R. S. & FOWLER, V. M. 2008. Thin filament length regulation in striated muscle
1139 sarcomeres: pointed-end dynamics go beyond a nebulin ruler. *Semin Cell Dev Biol,* 19**,**
1140 511-9.

1141 LIVAK, K. J. & SCHMITTGEN, T. D. 2001. Analysis of relative gene expression data using
1142 real-time quantitative PCR and the 2(-Delta Delta C(T)) Method. *Methods,* 25**,** 402-8.
1143 LOVE, M. I., HUBER, W. & ANDERS, S. 2014. Moderated estimation of fold change and
1144 dispersion for RNA-seq data with DESeq2. *Genome Biol,* 15**,** 550.
1145 MANHART, A., WINDNER, S., BAYLIES, M. & MOGILNER, A. 2018. Mechanical positioning
1146 of multiple nuclei in muscle cells. *PLoS Comput Biol,* 14**,** e1006208.
1147 MARDAHL-DUMESNIL, M. & FOWLER, V. M. 2001. Thin filaments elongate from their pointed
1148 ends during myofibril assembly in Drosophila indirect flight muscle. *J Cell Biol,* 155**,** 1043-
1149 53.
1150 MARTINO, F., PERESTRELO, A. R., VINARSKY, V., PAGLIARI, S. & FORTE, G. 2018.
1151 Cellular Mechanotransduction: From Tension to Function. *Front Physiol,* 9**,** 824.
1152 METZGER, T., GACHE, V., XU, M., CADOT, B., FOLKER, E. S., RICHARDSON, B. E.,
1153 GOMES, E. R. & BAYLIES, M. K. 2012. MAP and kinesin-dependent nuclear positioning
1154 is required for skeletal muscle function. *Nature,* 484**,** 120-4.
1155 MOHAMMAD, I., ARORA, P. D., NAGHIBZADEH, Y., WANG, Y., LI, J., MASCARENHAS, W.,
1156 JANMEY, P. A., DAWSON, J. F. & MCCULLOCH, C. A. 2012. Flightless I is a focal
1157 adhesion-associated actin-capping protein that regulates cell migration. *FASEB J,* 26**,**
1158 3260-72.
1159 MOLNAR, I., MIGH, E., SZIKORA, S., KALMAR, T., VEGH, A. G., DEAK, F., BARKO, S.,
1160 BUGYI, B., ORFANOS, Z., KOVACS, J., JUHASZ, G., VARO, G., NYITRAI, M.,
1161 SPARROW, J. & MIHALY, J. 2014. DAAM is required for thin filament formation and
1162 Sarcomerogenesis during muscle development in Drosophila. *PLoS Genet,* 10**,**
1163 e1004166.
1164 MORGAN, M., ANDERS, S., LAWRENCE, M., ABOYOUN, P., PAGES, H. & GENTLEMAN,
1165 R. 2009. ShortRead: a bioconductor package for input, quality assessment and
1166 exploration of high-throughput sequence data. *Bioinformatics,* 25**,** 2607-8.
1167 ONO, S. 2010. Dynamic regulation of sarcomeric actin filaments in striated muscle.
1168 *Cytoskeleton (Hoboken),* 67**,** 677-92.
1169 OTTENHEIJM, C. A., WITT, C. C., STIENEN, G. J., LABEIT, S., BEGGS, A. H. & GRANZIER,
1170 H. 2009. Thin filament length dysregulation contributes to muscle weakness in nemaline
1171 myopathy patients with nebulin deficiency. *Hum Mol Genet,* 18**,** 2359-69.
1172 PARDEE, J. D., SIMPSON, P. A., STRYER, L. & SPUDICH, J. A. 1982. Actin filaments
1173 undergo limited subunit exchange in physiological salt conditions. *J Cell Biol,* 94**,** 316-24.

1174 PARDO, J. V., SILICIANO, J. D. & CRAIG, S. W. 1983. A vinculin-containing cortical lattice in
1175 skeletal muscle: transverse lattice elements ("costameres") mark sites of attachment
1176 between myofibrils and sarcolemma. *Proc Natl Acad Sci U S A,* 80**,** 1008-12.
1177 PARSONS, J. T., HORWITZ, A. R. & SCHWARTZ, M. A. 2010. Cell adhesion: integrating
1178 cytoskeletal dynamics and cellular tension. *Nat Rev Mol Cell Biol,* 11**,** 633-43.
1179 PERKINS, L. A., HOLDERBAUM, L., TAO, R., HU, Y., SOPKO, R., MCCALL, K., YANG-
1180 ZHOU, D., FLOCKHART, I., BINARI, R., SHIM, H. S., MILLER, A., HOUSDEN, A., FOOS,
1181 M., RANDKELV, S., KELLEY, C., NAMGYAL, P., VILLALTA, C., LIU, L. P., JIANG, X.,
1182 HUAN-HUAN, Q., WANG, X., FUJIYAMA, A., TOYODA, A., AYERS, K., BLUM, A.,
1183 CZECH, B., NEUMULLER, R., YAN, D., CAVALLARO, A., HIBBARD, K., HALL, D.,
1184 COOLEY, L., HANNON, G. J., LEHMANN, R., PARKS, A., MOHR, S. E., UEDA, R.,
1185 KONDO, S., NI, J. Q. & PERRIMON, N. 2015. The Transgenic RNAi Project at Harvard
1186 Medical School: Resources and Validation. *Genetics,* 201**,** 843-52.
1187 PINES, M., DAS, R., ELLIS, S. J., MORIN, A., CZERNIECKI, S., YUAN, L., KLOSE, M.,
1188 COOMBS, D. & TANENTZAPF, G. 2012. Mechanical force regulates integrin turnover in
1189 Drosophila in vivo. *Nat Cell Biol,* 14**,** 935-43.
1190 QUACH, N. L. & RANDO, T. A. 2006. Focal adhesion kinase is essential for costamerogenesis
1191 in cultured skeletal muscle cells. *Dev Biol,* 293**,** 38-52.
1192 RAO, J. N., MADASU, Y. & DOMINGUEZ, R. 2014. Mechanism of actin filament pointed-end
1193 capping by tropomodulin. *Science,* 345**,** 463-7.
1194 ROMERO, N. B. 2010. Centronuclear myopathies: a widening concept. *Neuromuscul Disord,*
1195 20**,** 223-8.
1196 ROPER, K., MAO, Y. & BROWN, N. H. 2005. Contribution of sequence variation in Drosophila
1197 actins to their incorporation into actin-based structures in vivo. *J Cell Sci,* 118**,** 3937-48.
1198 ROSS, J. A., LEVY, Y., RIPOLONE, M., KOLB, J. S., TURMAINE, M., HOLT, M., LINDQVIST,
1199 J., CLAEYS, K. G., WEIS, J., MONFORTE, M., TASCA, G., MOGGIO, M., FIGEAC, N.,
1200 ZAMMIT, P. S., JUNGBLUTH, H., FIORILLO, C., VISSING, J., WITTING, N., GRANZIER,
1201 H., ZANOTELI, E., HARDEMAN, E. C., WALLGREN-PETTERSSON, C. & OCHALA, J.
1202 2019. Impairments in contractility and cytoskeletal organisation cause nuclear defects in
1203 nemaline myopathy. *Acta Neuropathol,* 138**,** 477-495.
1204 SANGER, J. M. & SANGER, J. W. 2008. The dynamic Z bands of striated muscle cells. *Sci*
1205 *Signal,* 1**,** pe37.
1206 SCHIAFFINO, S., DYAR, K. A., CICILIOT, S., BLAAUW, B. & SANDRI, M. 2013. Mechanisms
1207 regulating skeletal muscle growth and atrophy. *FEBS J,* 280**,** 4294-314.

1208 SCHMITTGEN, T. D. & LIVAK, K. J. 2008. Analyzing real-time PCR data by the comparative
1209 C(T) method. *Nat Protoc,* 3**,** 1101-8.
1210 SCHNORRER, F., SCHONBAUER, C., LANGER, C. C., DIETZL, G., NOVATCHKOVA, M.,
1211 SCHERNHUBER, K., FELLNER, M., AZARYAN, A., RADOLF, M., STARK, A.,
1212 KELEMAN, K. & DICKSON, B. J. 2010. Systematic genetic analysis of muscle
1213 morphogenesis and function in Drosophila. *Nature,* 464**,** 287-91.
1214 SEWRY, C. A., LAITILA, J. M. & WALLGREN-PETTERSSON, C. 2019. Nemaline myopathies:
1215 a current view. *J Muscle Res Cell Motil*.
1216 SHATTIL, S. J., KIM, C. & GINSBERG, M. H. 2010. The final steps of integrin activation: the
1217 end game. *Nat Rev Mol Cell Biol,* 11**,** 288-300.
1218 SHIRINIAN, M., POPOVIC, M., GRABBE, C., VARSHNEY, G., HUGOSSON, F., BOS, H.,
1219 REHMANN, H. & PALMER, R. H. 2010. The Rap1 guanine nucleotide exchange factor
1220 C3G is required for preservation of larval muscle integrity in Drosophila melanogaster.
1221 *PLoS One,* 5**,** e9403.
1222 SMILLIE, L. B. 1982. Preparation and identification of alpha- and beta-tropomyosins. *Methods*
1223 *Enzymol,* 85 Pt B**,** 234-41.
1224 SPARROW, J. C. & SCHOCK, F. 2009. The initial steps of myofibril assembly: integrins pave
1225 the way. *Nat Rev Mol Cell Biol,* 10**,** 293-8.
1226 SPLETTER, M. L., BARZ, C., YEROSLAVIZ, A., SCHONBAUER, C., FERREIRA, I. R.,
1227 SAROV, M., GERLACH, D., STARK, A., HABERMANN, B. H. & SCHNORRER, F. 2015.
1228 The RNA-binding protein Arrest (Bruno) regulates alternative splicing to enable myofibril
1229 maturation in Drosophila flight muscle. *EMBO Rep,* 16**,** 178-91.
1230 SPLETTER, M. L., BARZ, C., YEROSLAVIZ, A., ZHANG, X., LEMKE, S. B., BONNARD, A.,
1231 BRUNNER, E., CARDONE, G., BASLER, K., HABERMANN, B. H. & SCHNORRER, F.
1232 2018. A transcriptomics resource reveals a transcriptional transition during ordered
1233 sarcomere morphogenesis in flight muscle. *Elife,* 7.
1234 STEELE-STALLARD, H. B., PINTON, L., SARCAR, S., OZDEMIR, T., MAFFIOLETTI, S. M.,
1235 ZAMMIT, P. S. & TEDESCO, F. S. 2018. Modeling Skeletal Muscle Laminopathies Using
1236 Human Induced Pluripotent Stem Cells Carrying Pathogenic LMNA Mutations. *Front*
1237 *Physiol,* 9**,** 1332.
1238 SUSSMAN, M. A., BAQUE, S., UHM, C. S., DANIELS, M. P., PRICE, R. L., SIMPSON, D.,
1239 TERRACIO, L. & KEDES, L. 1998. Altered expression of tropomodulin in cardiomyocytes
1240 disrupts the sarcomeric structure of myofibrils. *Circ Res,* 82**,** 94-105.

1241 SWEENEY, H. L. & HAMMERS, D. W. 2018. Muscle Contraction. *Cold Spring Harb Perspect*
1242 *Biol,* 10.
1243 SZIKORA, S., GOROG, P. & MIHALY, J. 2022. The Mechanisms of Thin Filament Assembly
1244 and Length Regulation in Muscles. *Int J Mol Sci,* 23.
1245 TALBOT, J. & MAVES, L. 2016. Skeletal muscle fiber type: using insights from muscle
1246 developmental biology to dissect targets for susceptibility and resistance to muscle
1247 disease. *Wiley Interdiscip Rev Dev Biol,* 5**,** 518-34.
1248 TUBRIDY, N., FONTAINE, B. & EYMARD, B. 2001. Congenital myopathies and congenital
1249 muscular dystrophies. *Curr Opin Neurol,* 14**,** 575-82.
1250 VERHEYEN, E. M. & COOLEY, L. 1994. Profilin mutations disrupt multiple actin-dependent
1251 processes during Drosophila development. *Development,* 120**,** 717-28.
1252 VISA, N. & PERCIPALLE, P. 2010. Nuclear functions of actin. *Cold Spring Harb Perspect Biol,*
1253 2**,** a000620.
1254 WANG, W., LUO, J. & CARROLL, T. 2022. Rfastp: An Ultra-Fast and All-in-One Fastq
1255 Preprocessor (Quality Control, Adapter, low quality and polyX trimming) and UMI
1256 Sequence Parsing). R package version 1.6.0. ed.
1257 WEBER, A., PENNISE, C. R., BABCOCK, G. G. & FOWLER, V. M. 1994. Tropomodulin caps
1258 the pointed ends of actin filaments. *J Cell Biol,* 127**,** 1627-35.
1259 WEITKUNAT, M., KAYA-COPUR, A., GRILL, S. W. & SCHNORRER, F. 2014. Tension and
1260 force-resistant attachment are essential for myofibrillogenesis in Drosophila flight muscle.
1261 *Curr Biol,* 24**,** 705-16.
1262 WICKHAM, H. 2016. ggplot2: Elegant Graphics for Data Analysis.: Springer-Verlag New York.
1263 WILLIAMS, P. E. & GOLDSPINK, G. 1971. Longitudinal growth of striated muscle fibres. *J Cell*
1264 *Sci,* 9**,** 751-67.
1265 WINDNER, S. E., MANHART, A., BROWN, A., MOGILNER, A. & BAYLIES, M. K. 2019.
1266 Nuclear Scaling Is Coordinated among Individual Nuclei in Multinucleated Muscle Fibers.
1267 *Dev Cell,* 49**,** 48-62 e3.
1268 WINTER, J. M., JOUREAU, B., LEE, E. J., KISS, B., YUEN, M., GUPTA, V. A., PAPPAS, C.
1269 T., GREGORIO, C. C., STIENEN, G. J., EDVARDSON, S., WALLGREN-PETTERSSON,
1270 C., LEHTOKARI, V. L., PELIN, K., MALFATTI, E., ROMERO, N. B., ENGELEN, B. G.,
1271 VOERMANS, N. C., DONKERVOORT, S., BONNEMANN, C. G., CLARKE, N. F.,
1272 BEGGS, A. H., GRANZIER, H. & OTTENHEIJM, C. A. 2016. Mutation-specific effects on
1273 thin filament length in thin filament myopathy. *Ann Neurol,* 79**,** 959-69.

1274 YAMASHIRO, S., GOKHIN, D. S., KIMURA, S., NOWAK, R. B. & FOWLER, V. M. 2012.
1275 Tropomodulins: pointed-end capping proteins that regulate actin filament architecture in
1276 diverse cell types. *Cytoskeleton (Hoboken),* 69**,** 337-70.
1277 YAMASHIRO, S., GOKHIN, D. S., SUI, Z., BERGERON, S. E., RUBENSTEIN, P. A. &
1278 FOWLER, V. M. 2014. Differential actin-regulatory activities of Tropomodulin1 and
1279 Tropomodulin3 with diverse tropomyosin and actin isoforms. *J Biol Chem,* 289**,** 11616-
1280 11629.
1281 YAMASHIRO, S., SPEICHER, K. D., SPEICHER, D. W. & FOWLER, V. M. 2010. Mammalian
1282 tropomodulins nucleate actin polymerization via their actin monomer binding and filament
1283 pointed end-capping activities. *J Biol Chem,* 285**,** 33265-33280.
1284 YOUNG, M. D., WAKEFIELD, M. J., SMYTH, G. K. & OSHLACK, A. 2010. Gene ontology
1285 analysis for RNA-seq: accounting for selection bias. *Genome Biol,* 11**,** R14.
1286 YUEN, M., SANDARADURA, S. A., DOWLING, J. J., KOSTYUKOVA, A. S., MOROZ, N.,
1287 QUINLAN, K. G., LEHTOKARI, V. L., RAVENSCROFT, G., TODD, E. J., CEYHAN-
1288 BIRSOY, O., GOKHIN, D. S., MALUENDA, J., LEK, M., NOLENT, F., PAPPAS, C. T.,
1289 NOVAK, S. M., D'AMICO, A., MALFATTI, E., THOMAS, B. P., GABRIEL, S. B., GUPTA,
1290 N., DALY, M. J., ILKOVSKI, B., HOUWELING, P. J., DAVIDSON, A. E., SWANSON, L.
1291 C., BROWNSTEIN, C. A., GUPTA, V. A., MEDNE, L., SHANNON, P., MARTIN, N., BICK,
1292 D. P., FLISBERG, A., HOLMBERG, E., VAN DEN BERGH, P., LAPUNZINA, P.,
1293 WADDELL, L. B., SLOBODA, D. D., BERTINI, E., CHITAYAT, D., TELFER, W. R.,
1294 LAQUERRIERE, A., GREGORIO, C. C., OTTENHEIJM, C. A., BONNEMANN, C. G.,
1295 PELIN, K., BEGGS, A. H., HAYASHI, Y. K., ROMERO, N. B., LAING, N. G., NISHINO, I.,
1296 WALLGREN-PETTERSSON, C., MELKI, J., FOWLER, V. M., MACARTHUR, D. G.,
1297 NORTH, K. N. & CLARKE, N. F. 2014. Leiomodin-3 dysfunction results in thin filament
1298 disorganization and nemaline myopathy. *J Clin Invest,* 124**,** 4693-708.
1299 ZHENG, Y., BUCHWALTER, R. A., ZHENG, C., WIGHT, E. M., CHEN, J. V. & MEGRAW, T.
1300 L. 2020. A perinuclear microtubule-organizing centre controls nuclear positioning and
1301 basement membrane secretion. *Nat Cell Biol,* 22**,** 297-309.
1302